3-23-2018

Pseudo Linear Hall Effect Thruster Characterization through Potential, Magnetic, and Optical Measurements

Braeden A. Sheets

PSEUDO LINEAR HALL EFFECT THRUSTER CHARACTERIZATTION THROUGH POTENTIAL, MAGNETIC, AND OPTICAL MEASUREMENTS

THESIS

Braeden A. Sheets, 2nd Lieutenant, USAF

AFIT-ENY-MS-18-M-293

DEPARTMENT OF THE AIR FORCE
AIR UNIVERSITY

AIR FORCE INSTITUTE OF TECHNOLOGY

Wright-Patterson Air Force Base, Ohio

AFIT-ENY-MS-18-M-293

Pseudo Linear Hall Effect Thruster Characterization Through Potential, Magnetic, and Optical Measurements

THESIS

Presented to the Faculty

Department of Aeronautics and Astronautics

Graduate School of Engineering and Management

Air Force Institute of Technology

Air University

Air Education and Training Command

In Partial Fulfillment of the Requirements for the

Degree of Master of Science in Astronautical Engineering

Braeden A. Sheets, BS

2nd Lieutenant, USAF

March 2018

AFIT-ENY-MS-18-M-293

Pseudo Linear Hall Effect Thruster Characterization Through Potential, Magnetic, and Optical Measurements

Braeden A. Sheets
2nd Lieutenant, USAF

Approved:

Carl Hartsfield, PhD (Chairman)	Date
Maj. David Liu, PhD (Member)	Date
William Hargus, PhD (Member)	Date

Abstract

Electric propulsion systems are a more mass efficient method for providing a change in velocity, ΔV, to on-orbit spacecraft, than their chemical counterparts. In comparison, electric systems generally have a much higher specific impulse, $I_{sp,}$ than chemical systems. One option within the realm of electric propulsion is Hall Effect Thrusters, which have moderately high specific impulse values. From their advent in the 1960s, Hall Effect Thrusters have been used for orbit station keeping, attitude control, and orbit transfer. Although the discharge cavity is conventionally circular, pseudo-linear or racetrack shaped cavities have been developed. Even though Hall thrusters have decades of flight heritage, there are still many plasma behavioral characteristics which are still unknown. Multiple non-intrusive measurement techniques were used to investigate plasma behavior both in the plume and in the channel of a pseudo linear Hall thruster. Through the visible emissions captured by a high-speed camera, breathing mode characteristics were induced and analyzed. Spoke structures were observed in only certain parts of the thruster channel. Additionally, the plume divergence was characterized by use of a Faraday probe along two axes of the thruster, indicating significantly different “keep out” regions for potential thruster use on spacecraft. Also, an irregularity was observed in the channel of the pseudo-linear thruster, which potentially could affect the lifespan of the thruster.

Acknowledgements

I would like to express my sincere appreciation to Dr. Carl Hartsfield for his support and guidance throughout the course of this thesis effort. I would like to thank Captain Sam Wright for his collaboration and teamwork in operating, troubleshooting, and sharing the AFIT vacuum chamber facility and equipment. Finally, I would like to thank Mr. Josh Dewitt, Mr. Michael Ranft, Mr. Philip Smith Jr, and Mr. Jamie Smith for their laboratory assistance and expertise.

In addition, I would like to acknowledge Dr. Christopher Rice and Dr. Michael Hawks for their expertise and collection of spectrometry data on an observed irregularity.

I would also like to acknowledge Dr. Mitat Birkan of the Air Force Office of Scientific Research for providing funding and support for this research.

Braeden A. Sheets

Table of Contents

Page

List of Figures

Page

List of Tables

Page

List of Symbols

Symbol	Definition
$A_{aperture}$	Area of Faraday probe aperture
$\vec{B}$	Magnetic field
$\vec{E}$	Electric field
e	Electron charge
ε_o	Permittivity of free space
F	Force
F_c	Centripetal force
g_o	Gravitational constant
I_{sp}	Specific Impulse
I_H	Hall current
I_i	Ion current
$I_{s,e}$	Electron saturation current
$I_{s,i}$	Ion saturation current
$I_{e,e}$	Electron emission current
$\boldsymbol{J}$	Current density
m	Mass
$\dot{m}$	Mass flow rate
m_{ion}	Ion mass
n_e	Electron number density
n_i	Ion number density
n_s	Species number density
η_T	Thruster efficiency
p	Momentum
ρ	Charge density in plasma
P_{in}	Input power
q	Charge
q_s	Species charge state

R	Resistance
r_L	Larmor radius
s	Species
T	Thrust
T_e	Electron temperature
μ_o	Permeability of free space
v	Velocity
v_e	Exhaust velocity
v_s	Species velocity
v_i	Ion velocity
v_{elec}	Electron velocity
$v_\perp$	Perpendicular velocity
V	Voltage
V_d	Discharge voltage
V_f	Floating potential
V_p	Plasma potential
w_c	Cyclotron frequency
Z	Charge state
ϕ	Electric potential

PSEUDO LINEAR HALL EFFECT THRUSTER CHARACTERIZATTION THROUGH POTENTIAL, MAGNETIC, AND OPTICAL MEASUREMENTS

I. Introduction

Background

The theory of using rocket propulsion systems for space exploration was first perceived in the early twentieth century by Konstantin Tsiolkovsky. Since then two primary types of propulsion systems have been used in space, either chemical or electric systems. Chemical systems create thrust by sparking a reaction between an oxidizer and a fuel source. In space, chemical propulsion comes in three forms: a solid kick motor, a chemical liquid bi-propellant system, or a liquid monopropellant. While both of these forms provide a significant amount of thrust, chemical systems are generally very insufficient in the ratio of thrust to the rate of use of propellant, specific impulse (I_{sp}). In addition, chemical systems often require relatively large components and amounts of propellant in order for the system to operate. These components include tanks to store the fuel and oxidizer, a combustion chamber for the chemical reaction to occur, a converging-diverging nozzle to accelerate the flow to achieve the desired thrust, as well as the plumbing components that are associated with ensuring the proper mixture of the propellant. After all these components are integrated into a spacecraft, they tend to take up a meaningful amount of space and mass on the spacecraft.

Space and mass on a spacecraft are highly valuable to the consumer. With increased amounts of volume unoccupied, they are able to add more components, which can increase reliability or add to the satellite's mission capabilities. With reductions in mass, consumers can save on launch costs since they increase with mass. The use of

electric propulsion systems provides this for consumers. In addition, electric propulsion provides the spacecraft the ability to start and stop thrust multiple times, however, these systems are generally not throttleable like chemical systems. This is due to the low magnitude of thrust being produced often in the 100s of mN, whereas chemical systems are in the 100-1000s of N ranges. This low thrust is typically accounted for by the electric system being able to run the thruster for months in duration as opposed to chemical systems only being able to sustain thrust in the minutes to hours range before running out of propellant. This makes electric propulsion very appealing for spacecraft manufacturers keeping their assets in a constant orbit.

Space propulsion is used in a variety of ways such as overcoming the perturbations experienced in orbit (station keeping); whether they are due to atmospheric drag, J2, third-body effects, or others. Also, space propulsion systems can be used to change the orbit or to inject the spacecraft into an interplanetary trajectory. With chemical systems the optimal advantage comes with the time savings seen when changing an orbit or escaping the gravitational pull of the Earth. However, they come at the cost of having large margins of propellant onboard. The efficiency of use in the propellant is correlated with the I_{sp} of the system; chemical systems tend to be in the range of 100-500 seconds, where electric systems range from the 100s-1000s of seconds.

The I_{sp} for Hall thrusters typically range from 1500-2000s, which is much higher than those of chemical systems. Hall thrusters have been around since the 1960s, and have been used for station keeping, attitude control, and orbit transfer [1]. In 1971, the Soviets first flew a pair of Hall thrusters called Stationary Plasma Thrusters on the Meteor satellite [1]. The first flight of a Hall thruster on a U.S. spacecraft was in 1998 on

the National Reconnaissance Office's Space Technology Experiment Satellite, however the thruster was still developed in Russia. The first U.S. company to provide flight Hall thruster technology for spacecraft was Busek, Inc. that flew on board the Air Force TacSat-2, that was launched in late 2006 [1]. As requirements for high I_{sp} with space and mass savings increase with the number of small satellites being flown, Hall thrusters will become more prevalent. This will require better modeling of their capabilities for better efficiency and potentially better packaging.

A basic understanding of how Hall effect thrusters operate will be useful since this research focuses on a Hall effect thruster. In figure 1, the typical layout of a Hall effect thruster is shown. This design features a cylindrical channel that contains an anode and gas propellant feeds at the back. Magnets surround the channel with the exterior and interior cylinder composed of opposing magnetic polarities, that creates a radial magnetic field ($\vec{B}$). Along the channel an axial electric field ($\vec{E}$) is applied, the interaction between these fields traps electrons. This causes the electrons to drift around the channel in the $\vec{E} \times \vec{B}$ direction, this generates ions from the gas propellant as it flows axially through the channel. The ions are expelled, at 10-20 km/s, from the channel due to the electric field from the anode to the cathode-potential plasma produced at the front of the thruster [1]. As technology for the thrusters improves and as the cost of space operations decreases, Hall thrusters could see increased presence on small satellites. Since they take up considerably less volume than their chemical propulsion counterparts and they provide reliable propulsion, Hall thrusters are a desirable source of propulsion on small satellites.

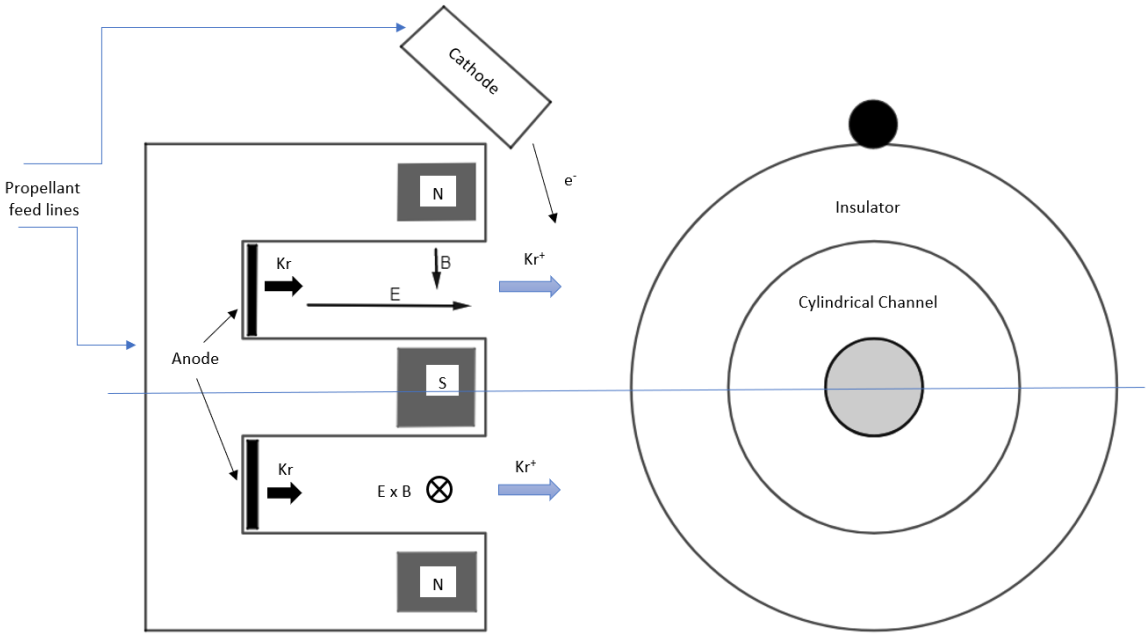

Figure 1: Typical Hall thruster schematic

Motivation

Although electric propulsion systems such as Hall thrusters have been around since the 1960s and have flight heritage dating back to 1971, understanding how they operate is still not complete. This is due to the complexities of the plasma dynamics in the thruster channel. As we learn more about their operation through research our goal will be to create more efficient thrusters with improved lifetimes, and to create more efficient models to predict plasma behavior. Current Hall thruster simulation models function adequately to capture accurate steady state thruster behavior (including the discharge potential and current), but they fail to capture dynamic thruster behavior at high data rates such as 500 kHz and higher [2].

The purpose of this research is to collect data from a 475 W pseudo linear Hall effect thruster at high data rates in a laboratory environment. The thruster will be

operated at steady state, in particular breathing and spoke modes, to compare with Hall thrusters of typical cylindrical geometry at similar power outputs. Also, to perform analysis on the data to correlate visual emissions with plasma potential measurements. In addition, the geometry of the pseudo linear (racetrack) design has several potential advantages relative to cylindrical thrusters including: linear scale up utilizing demonstrated cross section (reduced development cost), potential for higher performance, easier spacecraft integration including lower beam divergence, and significant thrust vectoring without gimbals [3].

Scope

The focus of this research will be to measure plume current density distribution, as well as high rate (500 kHz or higher) time correlated measurements of plasma potential, discharge current, and visible emission from a 475 W pseudo linear Hall thruster. These measurements will serve to determine the course of the investigation for the cause of noted preferential locations for apparent spoke initiation and also determine the path and distribution by which the spokes translate into the Hall thruster exhaust plume. Additionally, data will be analyzed to correlate behavior of plasma instabilities to determine causal relationships between plasma properties and anomalous diffusion modes.

Experimental Methodology

Experiments will be conducted in AFIT's Space Propulsion Application Simulation System (SPASS) laboratory. The vacuum chamber used will be a 3.75 m long by 1.8 m diameter cylinder that is capable of maintaining pressures on the order of 10^{-7}

torr with no gas flow into the chamber, or approximately $3 \cdot 10^{-5}$ torr with a medium size thruster operating.

During the experiments a 475 W pseudo linear Hall effect thruster will be mounted to a translational stand for testing. The ion current densities will be measured with a Faraday probe, swept through the plume on a multi-axis translation/rotation stage, the local plasma potential will be measured with an emissive probe, and visible emissions will be captured with a high-speed camera.

One area of interest is that the configuration of the pseudo-linear Hall Effect thruster is much different than the cylindrical thrusters used in the past with this chamber and the set-up from previous tests. Mounting the thruster in perpendicular configurations will be explored to determine the plume divergence characteristics of the design.

Experimental Results

Throughout the course of experiments, plasma instabilities will be induced by varying the discharge voltage and the current supplied to the magnets of the Hall thruster. From prior experiments on Hall thrusters, we expect to induce a breathing mode and observe spoke generation. However, due to the geometry difference of the thruster channel it is unclear if the results will be similar to those of cylindrical Hall thrusters. As the pseudo linear thruster is mounted in orthogonal orientations, it is expected that plume divergence will vary. With the thruster mounted the linear part of the channel parallel to the sweeping path of the Faraday probe, it is expected that the plume divergence will be much less than when the linear part of the channel is perpendicular to the sweeping path of the Faraday probe. Additionally, the methodology developed for the analysis of the data will provide insight into the inner workings of the Hall thruster. However, this

research will be made difficult by the lack of information and models of Hall thrusters at high data rates. As well as, the lack of information about differing Hall thruster geometries and the effects it has on the plasma; therefore, some of the data collected between the high data rates and differing geometry might not relate to something that is known.

Chapter Summary

In the first chapter a brief overview of the research was given which broken up into the background, motivation, scope, experimental methodology, and experimental result. In the chapters to come, the background, methodology, results, and conclusions will be discussed in further detail.

II. Background

Chapter Overview

This chapter will go through the fundamentals of rocket propulsion, the basics of plasma physics, operation theory of Hall thrusters, measurement techniques, and previous research on non-circular Hall thrusters and motivation. The purpose of this chapter is to provide the reader with an understanding of the theory and how relates to the experimental methodology and the results.

Fundamentals of Rocket Propulsion

Rocket propulsion is based on derivations from Newton's second law; which states that the sum of the forces on a system is equal to the time rate of change of the momentum.

$$\sum \mathbf{F} = \dot{\mathbf{p}} \tag{1}$$

Where **F** is the force and **p** is the momentum of the system. Momentum is the product of the systems mass (m) and velocity (v). When examining a rocket in a closed system, without the presence of external force, it begins with the assumption of conservation of momentum. Thus, the resulting acceleration of the spacecraft is due to the momentum exchange, as the spacecraft rocket expels mass at an exhaust velocity (v_e).

$$\mathbf{p} = mv = (m - dm)(v + dv) + dm(v - v_e) \tag{2}$$

Figure 2 depicts this system. By expanding these terms and neglecting the higher order terms we arrive at Eq. (3) and by expressing the terms over a change in time, dt, Eq. (4).

$$mdv = v_e dm \tag{3}$$

$$m\,{dv}/{dt} = v_e\,{dm}/{dt} = ma = -v_e\dot{m} \tag{4}$$

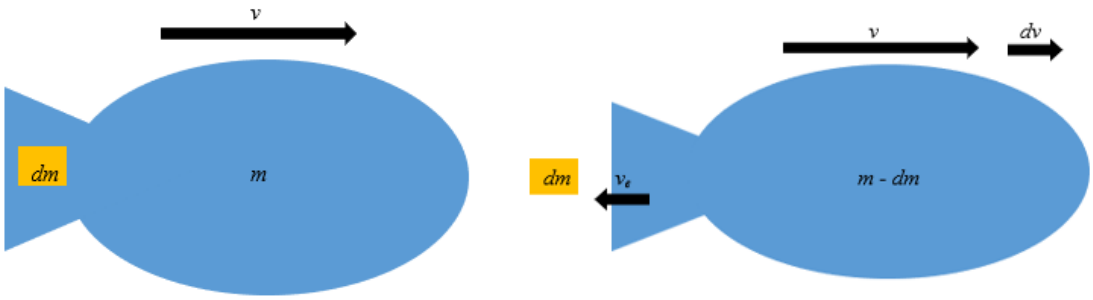

Figure 2: Ideal rocket

By combining equations (1) and (4), force is equal to the product of mass and acceleration, and the product of exhaust velocity and the mass flow rate ($\dot{m}$). This force is determined to be thrust (T)

$$T = v_e \dot{m} \tag{5}$$

Now if equation (3) is integrated, neglecting time dependence

$$\int_{v_o}^{v_f} dv = v_e \int_{m_o}^{m_f} \frac{dm}{m} \tag{6}$$

The result of the integration, returns equation (7),

$$v_f - v_o = \Delta v = v_e \ln\left(\frac{m_o}{m_f}\right) \tag{7}$$

exhaust velocity can be substituted by another performance factor, I_{sp}. When examining specific impulse, it is defined as the propellant effective exhaust velocity divided by the gravitational acceleration constant of Earth ($g_o = 9.8067\ m/s^2$) [1].

$$I_{sp} = \frac{v_e}{g_o} = \frac{T}{g_o \dot{m}} \tag{8}$$

Subsequently, this results in the ideal rocket equation in free space, equation (9).

$$\Delta v = I_{sp} g_o \ln\left(\frac{m_o}{m_f}\right) \tag{9}$$

The change in a space system's velocity as expressed in equation (9), is one of the key factors in quantifying the propulsion requirements for an orbital maneuver. Some propulsion systems rely on substantial changes in mass to produce large changes in velocity, others focus on higher exhaust velocities giving them higher I_{sp}s. Equations (5,8,9) enable the conversion from propulsion system performance in terms of I_{sp} and thrust to mission performance in terms of Δv available for a given propellant mass.

Basics of Plasma Physics

Plasma is a collection of the various charged particles that are free to move in response to fields; either those they generate or fields that are applied to the collection. These charged particles are produced by the ionization of a propellant gas, which creates both ions and electrons. Since both the ions and electrons come from the same neutral source, the collection is nearly electrically neutral. This means that the ion and electron densities are nearly equal, $n_i \approx n_e$, a condition commonly termed "quasi-neutrality" [1]. The assumption of quasi-neutrality is valid whenever the characteristic length of the plasma is much greater than the Debye length. The Debye length is the length in which mobile charge carriers screen out the external electric field, a measure of the shielding distance [4]. With the assumption of quasi-neutral plasma, many of the plasma conditions and responses in thrusters can be modeled by fluid equations, except for situations along the boundary of the plasma volume.

The electric and magnetic fields that are present in electric propulsion plasmas obey Maxwell's equations formulated in a vacuum that contains charges and currents [1].

$$\nabla \cdot \vec{E} = \frac{\rho}{\varepsilon_o} \tag{10}$$

$$\nabla \times \vec{E} = -\frac{\partial \vec{B}}{\partial t} \tag{11}$$

$$\nabla \cdot \vec{B} = 0 \tag{12}$$

$$\nabla \times \vec{B} = \mu_o \left(\boldsymbol{J} + \varepsilon_o \frac{\partial \vec{E}}{\partial t} \right) \tag{13}$$

Where ε_o is the permittivity of free space, ρ is the charge density of the plasma, μ_o is the permeability of free space, and $\boldsymbol{J}$ is the current density. The charge density and current density in these equations comprise all the charges and currents for the plasma. The plasma charge density is:

$$\rho = \sum_s q_s n_s = e(Zn_i - n_e) \tag{14}$$

where q_s and n_s are the charge state and number density, respectively, of species *s*; *e* is the chare of an electron; and *Z* is the charge state. The current density is:

$$\boldsymbol{J} = \sum_s q_s n_s v_s = e(Zn_i v_i - n_e v_{elec}) \tag{15}$$

where v_i, v_{elec}, and v_s are the velocities of the ions, electrons, and charge species, respectively. Also, for many types of electrostatic thrusters with static magnetic fields the electric field is defined as:

$$\vec{E} = -\nabla \phi \tag{16}$$

where the convention of the negative sign comes from the electric field pointing in the direction the ion motion, and ϕ is the electric potential.

An important topic to discuss in electrostatic thruster operation, in particular Hall thrusters, is examining single particle motion, as it will later relate to how the thrusters

operate. The motion for a charged particle moving in the presence of an electric and magnetic field is given by the Lorentz force equation.

$$\mathbf{F} = m\frac{d\vec{v}}{dt} = q\left(\vec{E} + \vec{v} \times \vec{B}\right) \tag{17}$$

Where *m* and *v* are the mass and velocity of the particle, and *q* is the charge of the particle. Consider the case of a charged particle moving in a uniform magnetic field, with the velocity perpendicular to the magnetic field. The Lorentz force becomes:

$$\mathbf{F} = qv_{\perp} \times \vec{B} \tag{18}$$

The force the particle feels will be a corresponding centripetal force, $\mathbf{F}_c$, as it moves circular orbit. Thus, by setting the forces equal to one another, the radius, r_L, of the orbit of the particle can be solved for, equation (20) [1].

$$\mathbf{F}_c = qv_{\perp} \times \vec{B} = \frac{m{v_{\perp}}^2}{r_L} \tag{19}$$

$$r_L = \frac{mv_{\perp}}{q\vec{B}} \tag{20}$$

This radius is known as the Larmor radius, and it is the radius that a particle will move as it moves along a helical path perpendicular to the electric and magnetic fields, as in a Hall thruster. With the Larmor radius and velocity of the particle, its cyclotron frequency, w_c, is:

$$w_c = \frac{v_{\perp}}{r_L} = \frac{q\vec{B}}{m} \tag{21}$$

Hall Thruster Operation Theory

Electrostatic propulsion is defined by the propellant being accelerated by direct application of electric body forces to ionized particles [5]. Hall thrusters although are

sometimes referred to as electromagnetic thrusters because of the magnetic field within the thruster. However, the magnetic field plays little role in accelerating the ionized propellant in comparison to the electrostatic field. The magnetic field nonetheless is an important factor in the ionization process. Figure 3 is a schematic of a coaxial Hall thruster; they are designed with a common channel, which the propellant flows through, around the center magnetic pole.

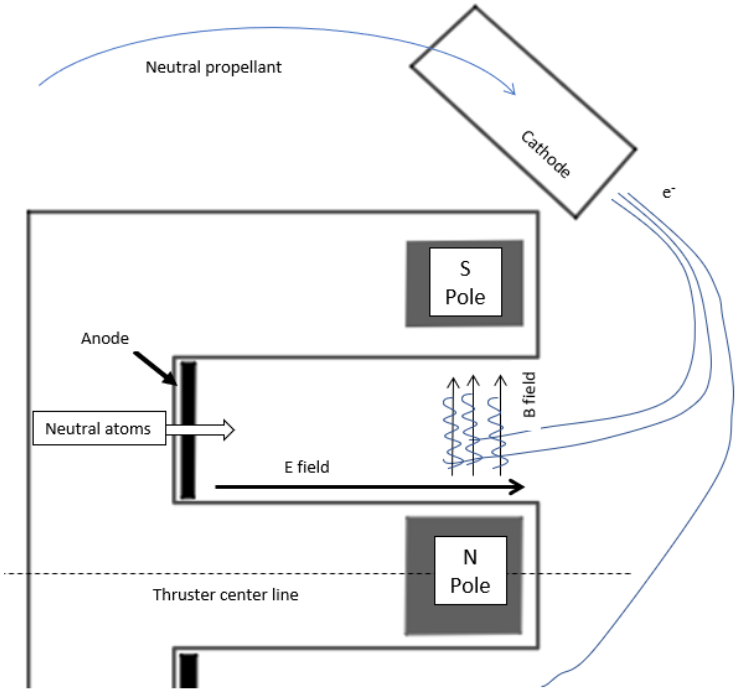

Figure 3: Hall thruster cutaway diagram

In order to operate the Hall thruster a power supply is used to apply a positive voltage to the anode, where the exit or cathode end of the channel is held at the ground potential, creating a difference in electrical potential axially. Additionally, to create the magnet field radially through the channel either permanent magnets or electromagnets are distributed around the channel's inner and outer walls.

The cathode plays a key role in the operation of the thruster, since it is the source of electrons needed to ionize the neutral gas propellant. These electrons are expelled from the cathode and are attracted to the positive charge of the anode. However, upon entering the channel, the Lorentz force generated by the electric and magnetic field causes the electrons to form a drift current in the $\vec{E} \times \vec{B}$ direction. While traveling along this path, the electrons also experience the helical motion defined by the Larmor radius. In order to ensure the electrons stay ideally trapped in the channel, the channel must be designed so that it is significantly larger than the Larmor radius to avoid collisions between the electrons and channel wall. In the conventional design of the hall thruster, the magnetic and electric field are always perpendicular, thus approximating the steady state case where the time derivative of velocity is zero:

$$\vec{E} = -\vec{v} \times \vec{B} \tag{22}$$

$$\overrightarrow{v_e} = \frac{\vec{E} \times \vec{B}}{B^2} \tag{23}$$

where v_e is the electron drift velocity around the channel, and assuming B and E are perpendicular $v_e=E/B$. This closed drift motion of electrons around the channel is referred to as the Hall current.

At the anode neutral atoms of the propellant are injected into the channel, once in the channel they encounter the region of high electron density. They are ionized due to the collisions with electrons moving about in the channel, once ionized they are propelled out of channel due to the electric potential in the channel. Unlike the electrons, the ions are not trapped in the channel by the Lorentz force due to their larger mass and size. After leaving the thruster channel, the ions are neutralized in the plume by electrons emitted

from the cathode. The electrons that impact the neutrals lose energy and gradually drift toward the anode. The electrons that are stripped from the neutrals become trapped in the Hall current and ionize more neutrals.

The thrust achieved in a Hall thruster can be calculated from the Hall current (I_H) and the magnetic field strength (B), or as a function of the ion current (I_i), ion mass (m_{ion}), and discharge voltage (V_d):

$$T = I_H B \approx I_i \sqrt{\frac{m_{ion} V_d}{2e}} \tag{24}$$

where e is the charge of an electron. Other performance factors to consider with the Hall thruster, include overall thruster efficiency, which is important for any propulsion system.

$$\eta_T = \frac{T v_e}{P_{in}} = \frac{T^2}{2\dot{m} P_{in}} \tag{25}$$

Where η_T is the thruster efficiency, P_{in} is the total input power, v_e is exhaust velocity, and $\dot{m}$ is the total mass flow to the anode and cathode. The total input power is a function of the discharge power, cathode keeper power, and the power required to operate the electromagnets.

When considering forms of space propulsion, it is necessary to be conscious of the potential life span of the system. This is typically an area where electrostatic propulsion is desirable, due to the low propellant densities and pressures in comparison to the chemical systems. Even though plasma temperatures are on the order of 100,000 K, there is very low heat transfer to the walls; due to very low density in the chamber plasma, convection to the wall is quite low. However, one area of concern for Hall thruster lifespan is the erosion of the thruster channel. This is caused by electron

collisions at the walls, typically the electron cloud will follow the $\vec{E} \times \vec{B}$ path around the channel. Occasionally, some of these electrons break free or are forced into the walls, impacting at several million meters per second. Thus, removing atoms or molecules from the wall insulation material, causing the insulator to eventually breakdown and alter the nominal operation of the Hall thruster.

During operation of the Hall thruster, instabilities in the channel and exhaust are often present. Although to the naked eye many of these instabilities go unnoticed, various measurement techniques have been used to reveal many kinds of oscillatory and unstable phenomena [6]. Even though there have been studies on these instabilities, research interest into them continues to be present due to the general lack of understanding in the underlying mechanism that are causing them and the effect that they have on thruster performance [7]. This lack of understanding heavily influences the development of thruster modeling to improve thruster design. Some of the instabilities present are the anomalous diffusion mode, breathing mode, spoke modes, and others exist, but they are outside the scope of the present research.

Anomalous Diffusion Mode

As the plasma tries to maintain it's quasi-neutrality some of the electrons will make their way to the anode. However, through measurements of the plasma, the electron current to the anode is higher than expected by classical diffusion theory [7,8,9]. The reason why anomalous diffusion is of interest is because when these modes are observed there appears to be a decrease in thruster efficiency, and increased erosion on thruster surfaces. These adverse effects ultimately shorten the life span of the thruster, thus shortening the lifespan of the spacecraft.

Breathing Mode

Breathing mode is the best understood mode of oscillation in Hall thrusters, generally this mode can be seen using high-speed imaging, resulting in cyclical increases and decreases in plume light emission intensity. A model developed by Boeuf and Garrigues [10], shows the instability is caused by a periodic depletion and replenishment of neutral atoms near the exit. This mode is generated by having a larger magnetic field in comparison to the electric field, than what is typically used for steady operations. With the large magnetic field ionization is enhanced and the neutrals become depleted. As the neutral density decreases the ionization decreases, causing the neutrals in the plume to move upstream until the ionization increases again. This process continues to oscillate, and thus resembles a breathing mode [6]. The model developed by Boeuf and Garrigues corroborates with the independent results of Fife *et. al* whose results resemble a predator prey model [11]. The completed cycle of the breathing mode will result in an oscillation whose frequency falls in the 15-22 kHz range [6]. As a note, this is pretty common in the best operating modes in Hall thrusters; where they are most efficient. It is also well correlated to the rate of "refilling" the ionization region, just from the mass flow of propellant into the thruster.

Spoke Mode

Spokes are a single major density fluctuation, in Hall thrusters these are designated by areas of increased electron density or ionization. The spokes in Hall thrusters were first observed by Janes and Lowder in 1966. These spokes travel along the channel in the $\vec{E} \times \vec{B}$ direction with cyclic frequencies in the 10-70 kHz range [7,9]. As a result of revolving around the channel, the spoke creates an azimuthal electric field

component driving electrons to the anode [12]. As discussed earlier, the interactions between electrons and the anode is not desirable, as it degrades the thruster, this drives the interest into a greater understanding of the mode.

Measurement Techniques

Three primary external instruments will be used to measure the plasma properties of the Hall thruster channel and exhaust plume; an emissive probe, a Faraday probe, and a high-speed imaging camera.

Emissive probes are used to measure the plasma potential of the moving plasma, the method used in this research was developed by Kemp and Sellen in 1966. Their method is based on letting the emissive probe potential float freely in relation to the laboratory ground by using a large load resistor [13]. In this case the floating potential of the probe is V_f, and this figure is used to determine the plasma potential V_p as illustrated in equation 26. With $I_{s,e}$, $I_{s,i}$, $I_{e,e}$ being the electron saturation current, ion saturation current, and electron emission current, respectively.

$$V_f = V_p - T_e \ln\left(\frac{I_{s,e}}{I_{s,i} + I_{e,e}}\right) \tag{26}$$

When the filament of the floating probe is sufficiently heated with a direct current power supply it enters the regime of electron emission. As the electron emission current is increased, the measured floating potential tends to approach the plasma potential as long as $ln(I_{s,e}/(I_{s,i} + I_{e,e}) > 1$. However, the two figures (V_f, V_p) are not exactly equal to one another due to the temperature of the emitted electrons will be less than the electron

temperature. Although, when only examining relative changes in V_p, V_f can be used as a good approximation for quantity change [13,14].

A Faraday probe is used to measure the ion current density within the plume of the electrostatic thruster exhaust. The standard Faraday probe is polarized negatively in order to repel electrons and solely collect ions. The ions collected by the probe create a current that can be measured to obtain the ion current density. Moving the probe through the entire ion beam allows obtaining the ion current density distribution [15].

The high-speed imaging camera is used to capture visible photon emission from the plasma of the Hall thruster at data rates up to one million frames per second. At these high data rates, the camera has the ability to capture some of the instability modes of the Hall thruster. The camera can be used in conjunction with other measurement techniques to create time correlated data for analysis.

Previous Research/Motivation

Previous research into electrostatic propulsion, in particular Hall thrusters, has primarily focused on conventional cylindrical channels. This research will focus on a non-circular channel design, which has also been referred to as racetrack, pseudo-linear, and obround, as shown in figure 4 below in comparison to the cylindrical design.

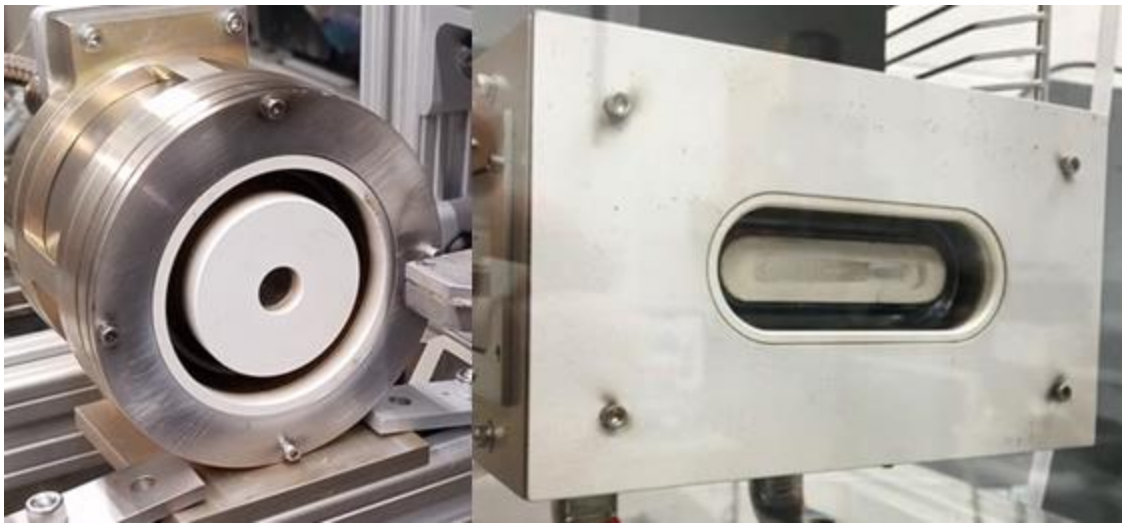

Figure 4: Channel Comparison Cylindrical (left), Pseudo Linear (right)

Since Hall thruster have typically been constructed in the cylindrical channel, and these designs have extensive flight history, few attempts have been made at altering the geometry of the channel. In the late 1990s, two non-circular designs came about, one being a straight linear channel [18], and the other being the racetrack design [17].

The racetrack design is built off of the circular design, and has several potential advantages over it, including linear scale up utilizing demonstrated cross section (reduced development cost), potential for higher performance, easier spacecraft integration including lower beam divergence, and significant thrust vectoring without gimbals [18]. However, the research available into these potential advantages is sparse, and through testing the racetrack design has shown similar performance outputs as to the circular design [17]. The motivation for this research is to gain a better understanding of pseudo-linear Hall thrusters and their instabilities, and with that knowledge improve design to increase performance and efficiency.

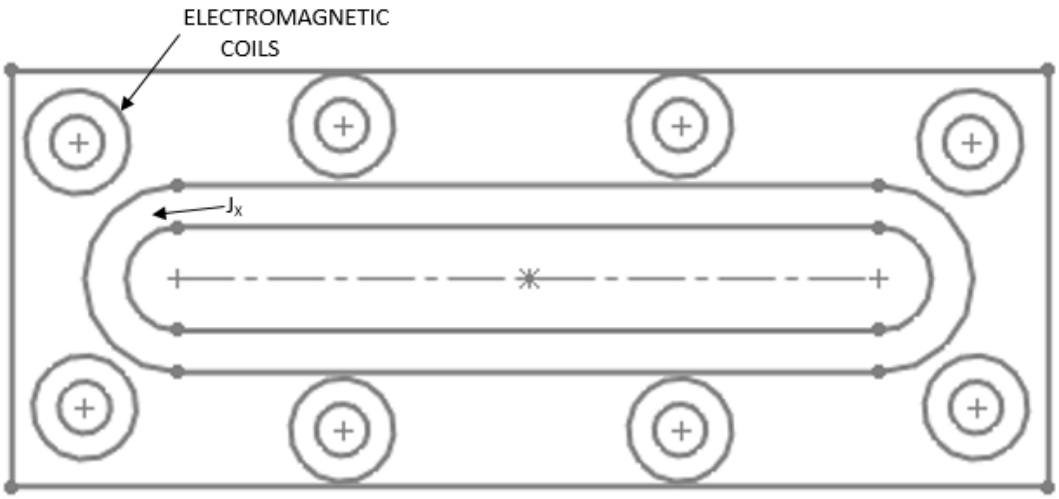

Figure 5: Frontal view of early developed racetrack Hall thruster

III. Experimental Setup and Methodology

Chapter Overview

This chapter will go through the lab facility and the equipment used to achieve to achieve desired testing conditions. The experimental setup is also described, to give future researchers the ability to duplicate the experiments and find corresponding results. In addition, the methodology in breaking down the data will be addressed.

Lab Facility

For this research, experiments were conducted in the Air Force Institute of Technology's Space Propulsion Application Simulation System (SPASS) laboratory. The SPASS lab vacuum chamber used is nearly cylindrical, including hemispherical doors, with an axial length of 3.75 meters and a 1.8 meter diameter, the approximate volume is 9.6 cubic meters. The chamber is capable of maintaining pressures less than or equal to $7x10^{-7}$ Torr, when no propellant gas is being flowed in. During thruster operations, the chamber maintains pressures in the range 10-50 microTorr. The chamber is able to achieve these pressures by utilizing multiple pumps programmed to effectively evacuate the chamber. First an Oerlikon/Leybold Vacuum Screwline SP 250 roughing pump is used to bring the chamber pressure down to approximately 70 milliTorr. Once the desired switchover pressure is achieved, four CVI Torr Master 20 inch TM500 helium cooled cryopumps and a final helium cooled cryo plate, mounted on the chamber ceiling downstream of the thruster, lower the chamber pressure to desired thruster operating conditions. Initially the chamber pressure is measured with a Pirani gage, however it becomes unreliable below the mTorr range and an ExTorr Residual Gas Analyzer is used to measure the pressure.

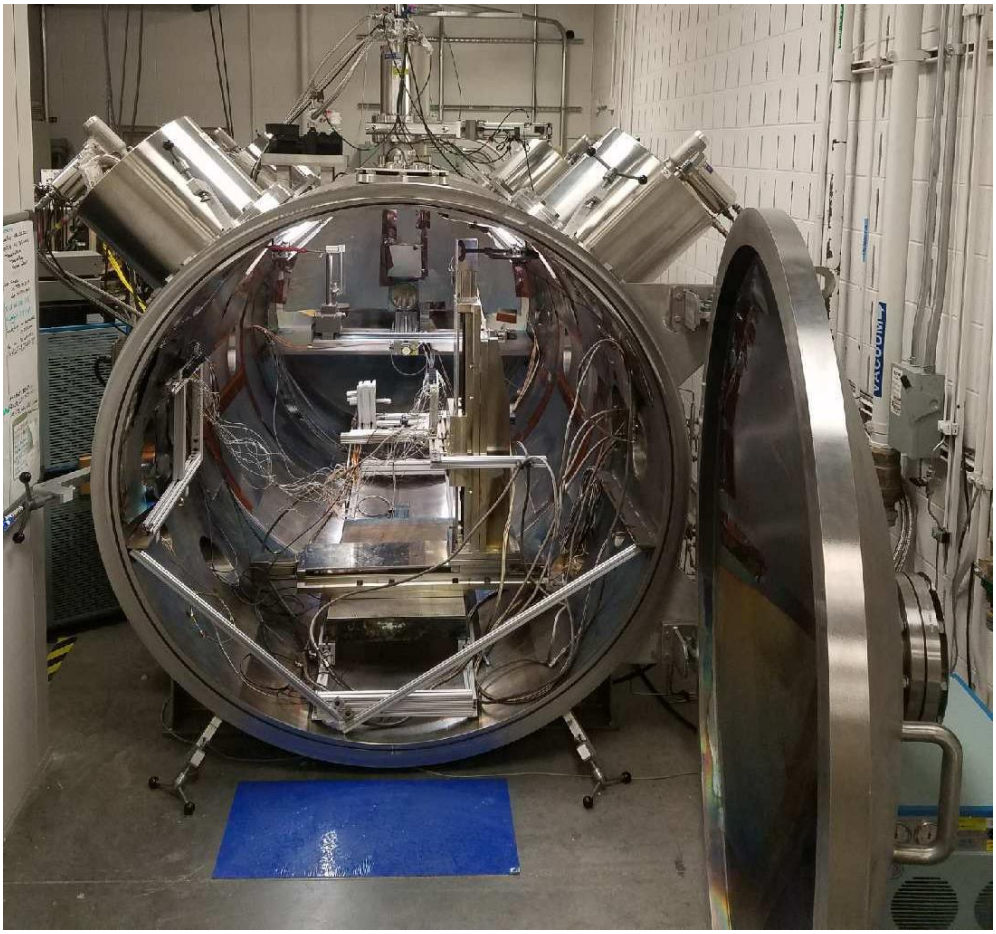

Figure 6: SPASS vacuum chamber

Around the chamber there are several ports that are affixed with quartz windows which allow for visual inspection of thruster operations when vacuum pressures have been achieved, as well as, allowing for high speed data collection.

Inside of the chamber there are three translational stands/devices used to position equipment. First, there is a rail system built with locks that spans approximately two thirds of the chamber length. This system can only be adjusted when the chamber is at atmospheric conditions, as it requires external input. The second translational stand is mounted to the rail system and allows for movement in the x,y,z directions, as seen in

figure 7. The Hall thrusters are mounted to this stand via a platform constructed out of 80/20 aluminum extrusions.

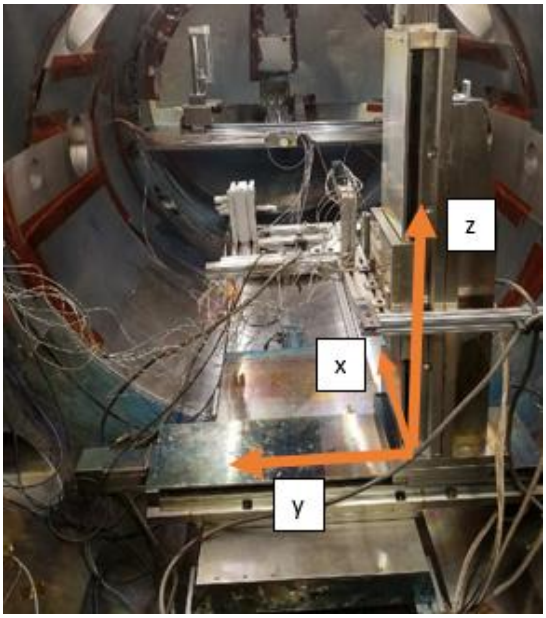

Figure 7: Thruster translation stand

Downstream from the thrusters there is the other translational stand, which can translate in the x and y directions in addition to rotating about the z axis, as shown in figure 8. This stand is useful, in that it allows for probes to be moved throughout the plume of the thruster without interfering with thruster operation.

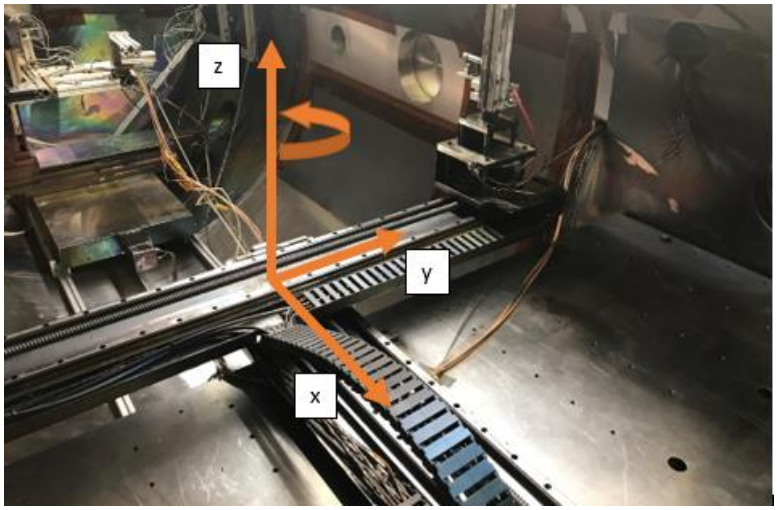

Figure 8: Probe translational stand

Prior to testing, the chamber had undergone an expansion which required ensuring all the seals were properly affixed. However, during pump down operations, it was noticed that the chamber was not reaching the desired pressures for thruster operations. During the trouble shooting of this issue, the Hall thrusters were unable to be fired due to potentially increased degradation effects associated with operating at relatively high pressure (above 1 mTorr). This issue was alleviated by ensuring all sensors to the pumps on the chamber were properly connected and the adjusting the crossover pressure between the roughing pump and the cryopumps.

Thruster Wiring set-up

The Hall thrusters and cathodes were connected to the power supplies outside the channel via a patch panel, shown in figure 9. This allowed for transferring of thruster operation between multiple thrusters being research without having to vent and re-pressurize the chamber.

Figure 9: Chamber patch panels interior (left), exterior (right)

The wiring diagram for the pseudo linear thruster is shown in figure 10, it is based on the Hoffman pass through wiring diagram. The cathode and the leads for the electromagnet

were connected to the interior patch panel shown in figure 9, while the lead for the anode was connected via a BNC connector to accommodate the high voltages being supplied.

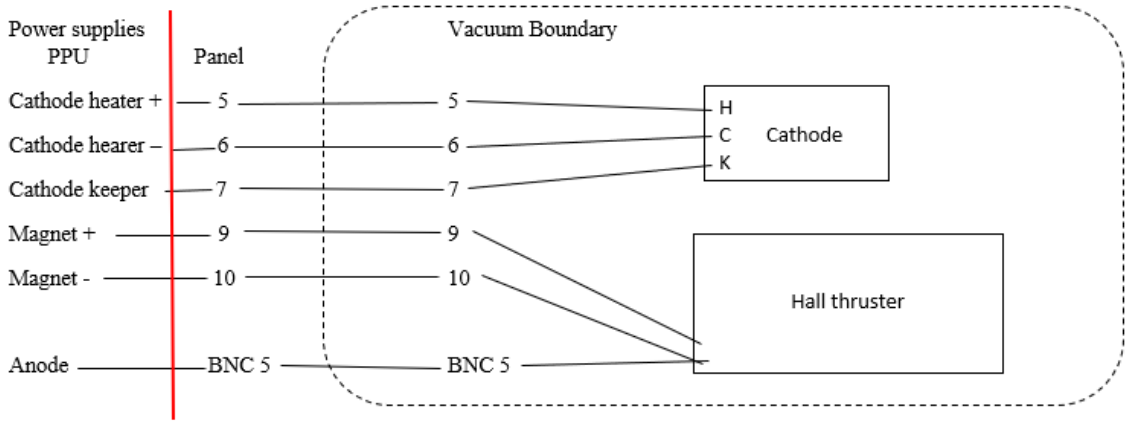

Figure 10: Wiring diagram

Thruster Equipment

The Hall thruster and hollow cathode that were used for the present research are a commercially sourced 475 watt electromagnet thruster designed and manufactured by Busek, BHT-400-OCD, and a Busek BHC-1500 cathode. This thruster has a nominal I_{sp} of 1399 s and thrust of 16.9 mN [19]. Hall thrusters with these ranges are typically employed on small satellites due to their level of thrust and power requirements to run the system. Comparing the manufacturer test data with that of cylindrical Hall thrusters of similar power requirements, the pseudo linear thruster is delivering approximately half the thrust and half the total thruster efficiency, with it being typically 20 percent efficient [21]. The power to operate the thruster is being supplied by a Sorensen DCS55-55E power supply and the power is regulated by a Power Processing Unit (PPU). The PPU and its associated software were designed by Busek, and allow the operator to control the inputs into the thruster, within designed limits.

Unlike the Hall thruster in this research, the cathode has had flight history; it has been used on the Operationally Responsive Space satellite TacSat-2 [22]. This cathode uses a porous tungsten hollow insert impregnated with a low work function emitter, a barium-calcium-aluminate mixture. A co-axial tantalum swaged heater wire is used to bring the emitter to ignition temperature of approximately 1000-1200°C. The cathode assembly incorporates an integral enclosed keeper to start the cathode and sustain an internal discharge before establishing thruster operation. The keeper also provides a radiation and sputter shield to protect the emitter from environmental damage [20]. In order to prevent the tungsten from oxidizing, which leads to inhibiting electron emission, the cathodes are kept in a nitrogen rich environment. The thruster is designed to operate with the cathode mounted to the thruster as seen in figure 11.

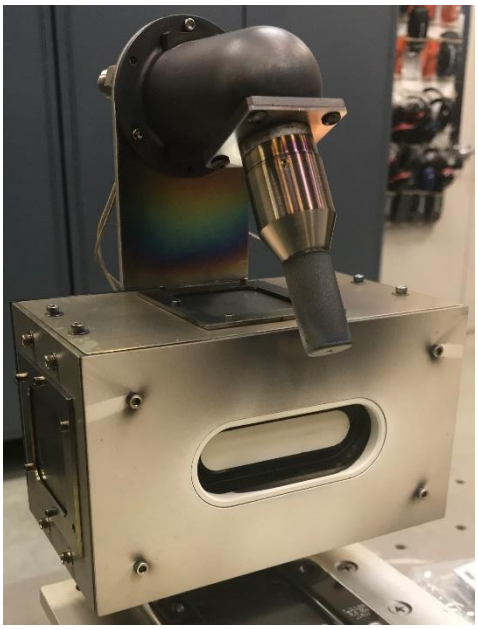

Figure 11: Racetrack Hall thruster and Cathode

The thruster has points on the back where a mount can be affixed that would hold the cathode in a fixed location to the thruster channel. However, this bracket, figure 12,

had to be custom made to accommodate the design of the thruster and cathode. As well as, position the cathode in an optimal location in relation to the thruster channel for operation. Initially, when the thruster was received the propellant feeds for the anode were not connected. Subsequently, plumbing was added to ensure even distribution of propellant in the channel. This was accomplished by combining the two feed lines into one with equal path lengths and geometry on each side.

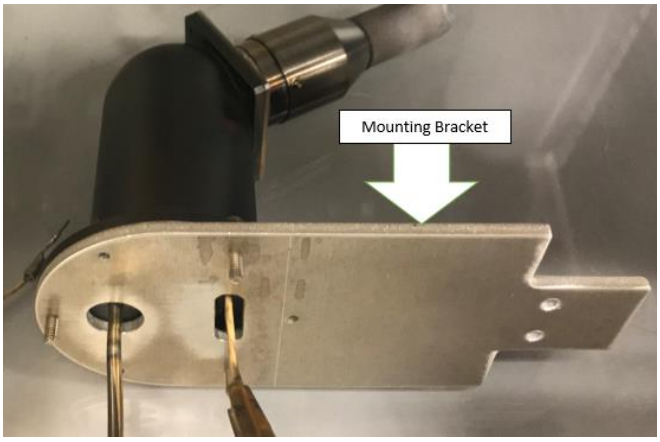

Figure 12: Cathode Mounting Bracket

Thruster propellant set-up

The propellant flow through the anode and cathode, are regulated by a mass flow controller. The controller allows the operator to vary the amount of propellant being supplied as a percentage of the flow allowed through that particular mass flow line's controller. The propellant is stored in tanks, in the current configuration the gases being stored are approximately 99.99% pure laboratory grade krypton and xenon. There are two control valves for each tank, one on the tank and one on the set-up, to ensure the gases are not mixing when the propellant types are switched. Typically, the krypton is stored with the pressure 200-300 psi greater than the xenon. After the propellant goes through

the controllers, it is feed into lines inside the vacuum, via a pass through mounted on the side of the chamber.

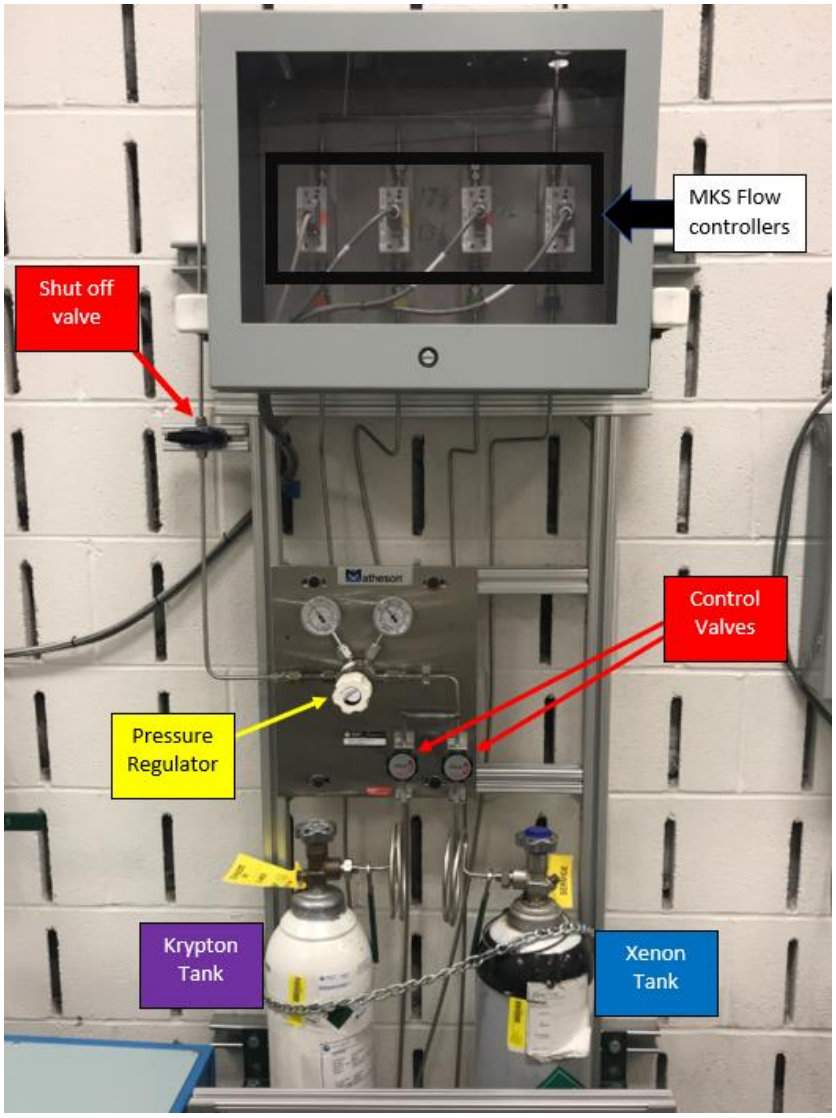

Figure 13: Propellant set-up

Thruster and Cathode Operation

Due to the chamber expansion and issues in the previous student's research, concerning the ability to get the thruster firing, getting the thruster to fire was the first goal of this research [23]. In order to get the thruster working the starting procedures

outlined in the operating manuals and steps modified from previous research were followed as indicated below [7,19,20]:

1. Introduce a mass flow of propellant to the cathode at 1.5 sccm
2. Begin initial cathode heating, apply 2 amps to cathode heater then wait 90 min
3. Increase cathode heater current to 4 amps, then wait 90 minutes
4. Increase cathode heater current to 6 amps, then wait 30 minutes
5. Apply 0.5 amps to the cathode keeper
   The cathode keeper will indicate a voltage around 600 volts until it ignites then it will indicate in the range of 30-40 volts
6. Once the cathode is ignited, the thruster can be fired
7. Introduce a mass flow to the anode at 10-15 sccm
8. Apply 1-2 amps of current to the magnets
9. Apply potential of 200 volts to the anode
10. Decrease the current to the magnets until the discharge ignites, then scale it back up (not to exceed 2.3 A)
11. Allow the thruster to run for about an hour, so it is able to outgas and stabilize
12. Decrease the cathode heater current to 0 amps
13. If the thruster is being restarted and has broken vacuum, the initial cathode heater current can be set up to 6.5 amps, there is no need to recondition unless exposed to atmosphere.

High Speed Imaging

The first set of data gathered for the experiment captured the visible emission of the plasma within the thruster channel. A Shimadzu Hyper Vision HPV-2 high-speed video camera with a 400 mm Nikkor lens was used to capture video of thruster operation. The camera and lens setup used for testing is shown in the Figure 14 below. In each recording, the HPV-2 captures 102 frames of 312 by 260 pixel images at rates up to 1 million frames per second (Mfps). The camera will have the f-stop set at its highest setting of f/2.4, to maximize the light incident on the complementary metal-oxide semiconductor (CMOS) sensor. Since the CMOS sensor is sensitive to emissions across the visible spectrum and Hall thruster emit excited ions, no additional lighting was used and ambient light from the lab was shielded from the lens. Since these settings allowed

for the least amount of light at the camera, the gain for the camera was increased to the max settings to enhance the usability for the images. Given the outputs from the camera program are panchromatic images, color will be added according to intensity to assist in post processing.

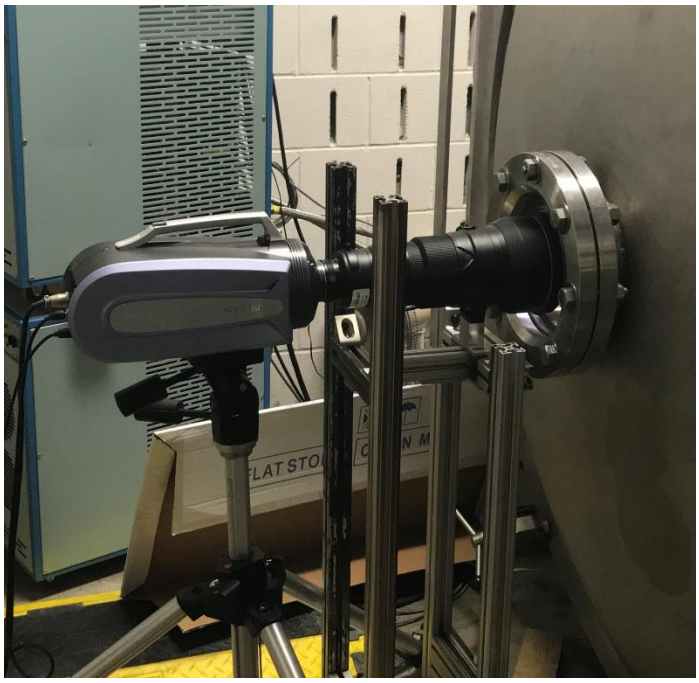

Figure 14: High speed camera set-up

Image analysis was conducted with Matlab®. The program read in the individual frames of the video and projected the area of the thruster channel to correlate with time for easier analysis. Built on work accomplished in previous research, the cylindrical thruster channel was unwrapped into a linear line segment, as shown in Figure 15 [7]. Since, the shape of the thruster channel in previous research was a circle, the geometry of unwrapping the channel is easier to visualize. For the unwrapping of the pseudo linear channel this would have to be accomplished in channel segments, and compiling the data into a vertical line afterwards. Figure 16 illustrates this process.

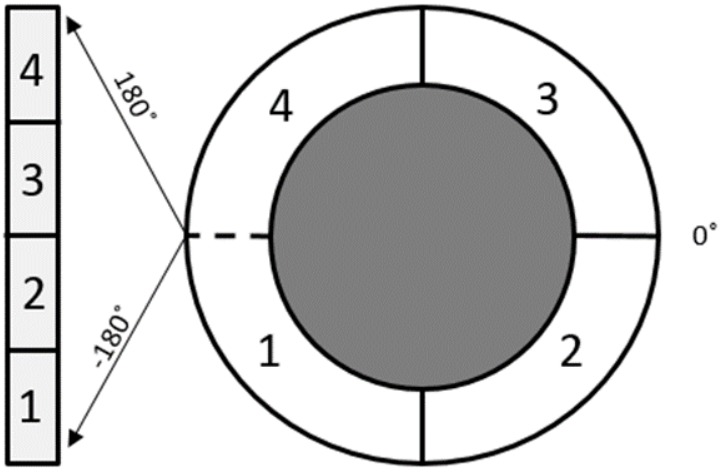

Figure 15: Schematic demonstration of cylindrical channel projection[23]

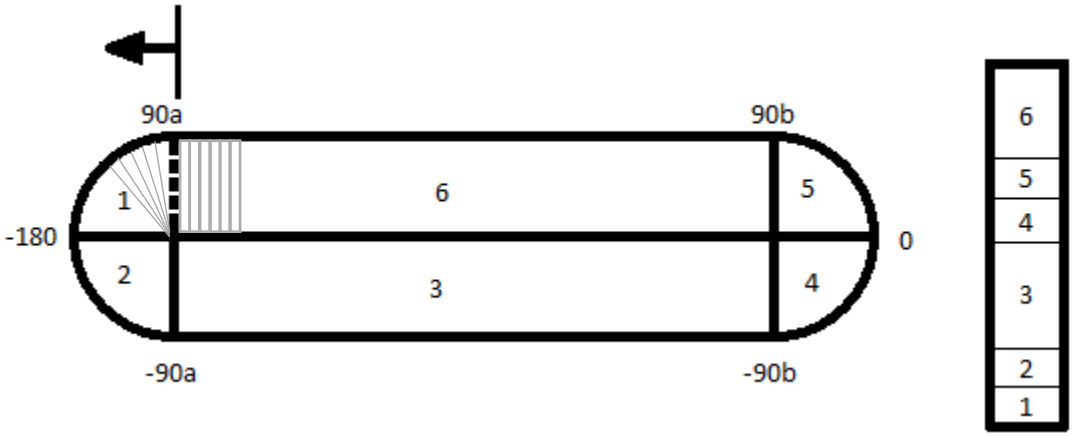

Figure 16: Schematic demonstration of pseudo linear channel projection

Although the schematic shows six segments being used, all the segments were broken down into smaller pieces, summing to a total of 936 pieces. The linear and curved portions remained at equal scaling in proportion to their arc lengths around the channel. Each vertical pixel row, either representing a 1 degree band around the turn or a linear segment equally spaced between the turns, as shown briefly in segments one and six.

These rows were compacted down to the average radially brightness, to primarily focus on the movement around the channel. Instead of each frame being represented by 936 rows and 180 different brightness columns, the new resultant frame is 1x936. Scaling is used to increase the widths of the frames to make the final image easier to visualize. This unwrapping and averaging was done for each of the 102 frames recorded per video. The frames are aligned sequentially from the left to show the progression in time of the channel brightness. False color was applied in the Matlab® program to allow for easier visual examination of the plasma structures [7]. Figure 17 shows an example of the output produced by the program for a cylindrical thruster using the schematic illustrated in Figure 15.

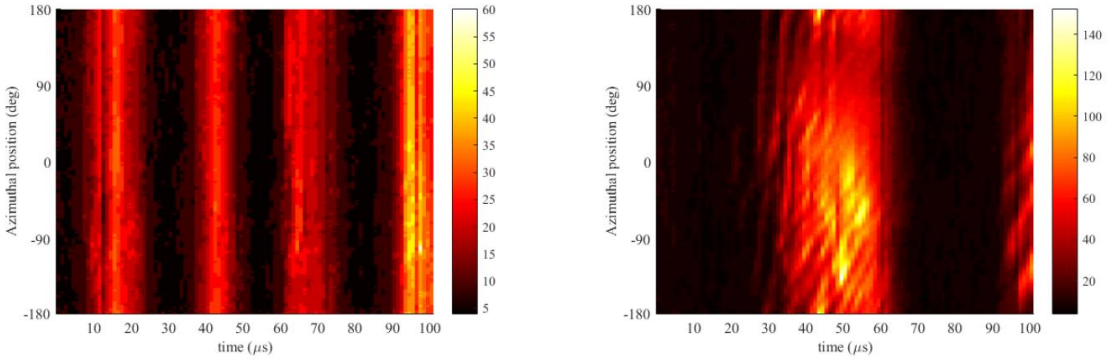

Figure 17: Example cylindrical channel plots [7]

The figure on the left, Figure 17a, illustrates the breathing mode of the cylindrical Hall thruster, with the red to white scale representing an increase in excited ions. The breathing is well defined by the oscillatory increase and decrease in ionization of the plasma. Figure 17a is similar to Figure 18a which shows an example of the projection plot of the pseudo-linear Hall thruster in an oscillating breathing mode. The figure on the right, Figure 17b, is examining the azimuthal spokes in the cylindrical Hall thruster exhaust, as noted by the intensity in the read outs moving in a steady pattern as time

progresses. Comparing Figure 17b with Figure 18b, the movement of the spokes in the pseudo-linear design is not as well defined as in cylindrical design. Similarly, the spokes in Figure 18b generally move in the counter clockwise, $\vec{E} \times \vec{B}$, direction as is depicted in Figure 17b and previous research. As a note, the bands seen in Figure 18 above -90a and 90b will be discussed later.

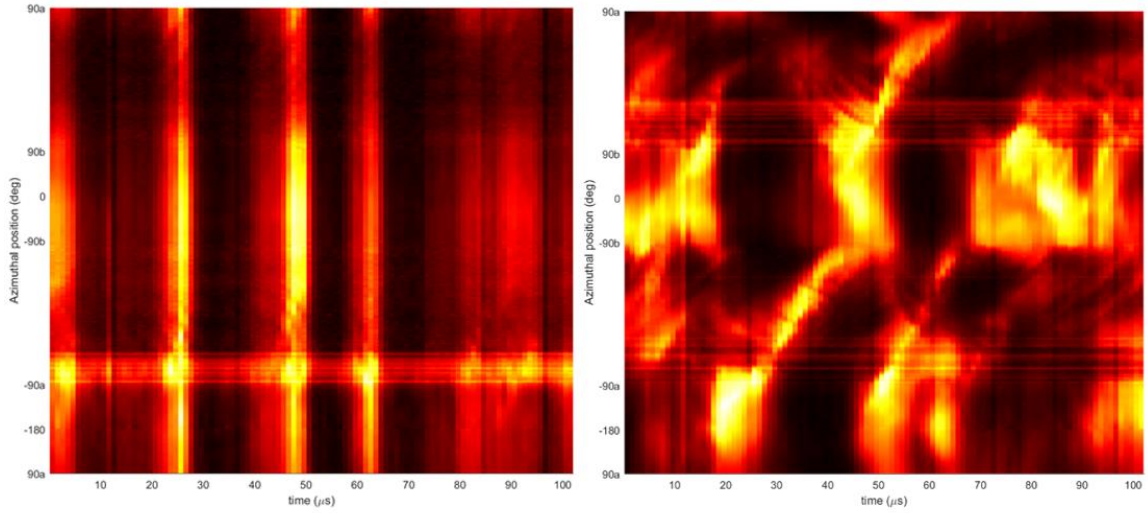

(a) Breathing mode (b) thruster in a quasi-spoke mode

Figure 18: Example Pseudo Linear channel plots

Emissive Probe

The emissive probe used for the current experiment was developed by Plasma Controls. The probe consists of an exposed 0.005 in piece of tungsten wire gently bent in to a u-shape, with the non-exposed ends of the tungsten crimped into copper tubes and the copper tubes inserted into a double bore alumina tube.

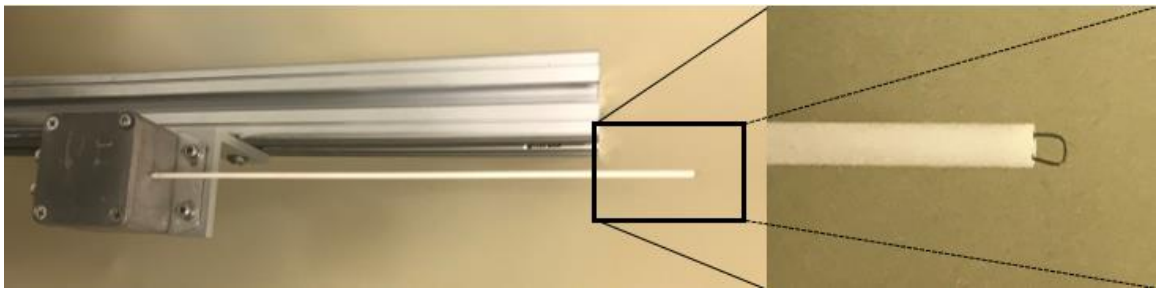

Figure 19: Emissive probe, tungsten wire loop (right)

The structure on the left in figure 19 was positioned inside the chamber, downstream of the thruster on the thruster translation stand, so that the thruster can move without disturbing the probe. This allowed for the probe to be positioned inside of the plume with the high-speed camera still focusing on the plasma in the channel. The probe is connected to the control unit outside of the chamber via two BNC connectors, as depicted in the wiring diagram.

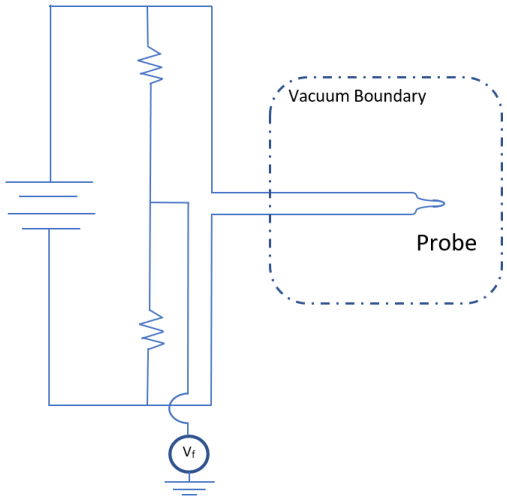

Figure 20: Emissive probe wiring diagram [24]

The emissive probe will be heated by a potential from a battery floating with the probe, while the floating potential is sampled across the resistor divider by a PicoScope. The data collection will be trigged from the oscilloscope, that is measuring the discharge of the thruster, using a transistor-transistor logic (TTL) pulse set to trigger at a desired

setting or on command. This same pulse will also trigger the high-speed camera to sample the thruster plasma. The data collection for the emissive probe will go through a data acquisition system (DAQ), that is operated by a Plasma Controls designed LabView program that filters and stores probe outputs. The trigger schematic for the time correlated data collection between the oscilloscope, emissive probe, and high-speed camera is illustrated in figure 20. In addition, based on previous research there is some timing uncertainty in this trigger mechanism that affects high speed data collection; HPV-2 camera ± 0.5μs, emissive probe ± 0.008μs [7].

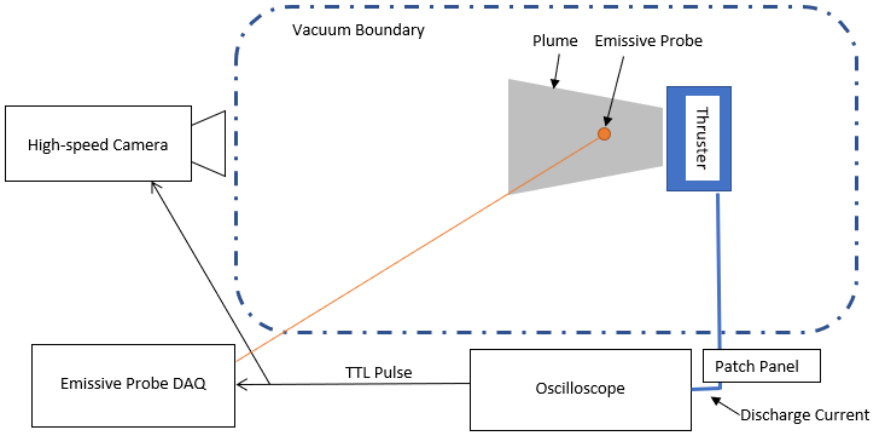

Figure 21: Trigger schematic

Faraday Probe

The Faraday probe used for the current experiment was developed by Plasma Controls. The probe consists of a collector disk that is shielded by the probe body, except for a small aperture, 0.015” in diameter. The probe is isolated from the mounting surface via a isolator mount, provided with the probe, and the probe is connected to the power supplies through a BNC connector [25]. The center wire of the BNC is electrically

connected to the collector plate, while the outside of the BNC cable is electrically connected to the body, as depicted in figure 22.

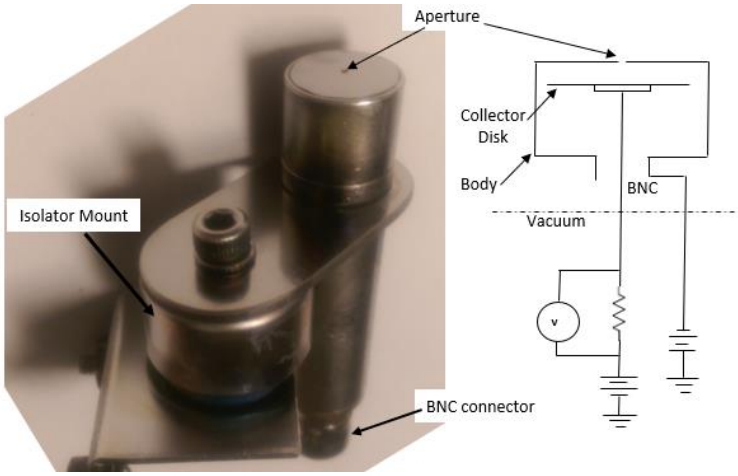

Figure 22: Faraday probe

Since the collector plate and body of the Faraday probe have separate electrical connections, this allowed for the collector plate to be biased to positive 30 volts and the body to be biased to negative 30 volts. These two potentials allow the collector plate to repel any low energy charge exchange ions that exist within the vacuum and the body to repel beam plasma electrons from reaching the collector plate. Also, the combination of these biases aids to eliminate secondary electron emission from the collector [25].

The measurements were collected by applying the biases to the probe, and setting the probe aperture channel to aim at the center of the plume. The ions from the plasma would then the enter the probe through the body aperture and collide into the collector disk, this imparts a current on the probe. The current is calculated by the measured voltage across a resistor that is placed electrically between the collector plate and ground, the current density (j_B), in μA/cm^2, is calculated according to equation 27:

$$j_B = \frac{V * 1E6}{R * A_{aperture}} \tag{27}$$

Where the resistor (R) used is 4.66 MΩ, the area of the aperture ($A_{aperture}$) is 0.00114 cm^2, and V is the recorded voltage.

During measurements, the Faraday probe works in harmony with the probe translation stand, figure 8, to collect data throughout the cross-sectional area of the plume. In order to take satisfactory measurements, it is preferable to have the aperture always aimed at the center of the plume, this was accomplished using a Plasma Controls developed LabView program. The program controls both the probe and the stand simultaneously, requiring minimal user inputs to adjust for the position of the thruster in relation to the stand. The program selected to take measurements in this research allows the Faraday probe to take measurements at intervals while the stand follows an arc of constant radius from the thruster while rotating the probe to point at the thruster. The program also allows for changing the increments of degrees in relation to the thruster in which the probe collects data, as well as setting an initial and final radius and the number of arcs desired to be measured in one run. Figure 23 shows the schematic used for the majority of collection, with the radius increasing in increments of 10 cm from 80 cm to 150 cm, as the probe is taking a measurement every 2.5 degree of arc.

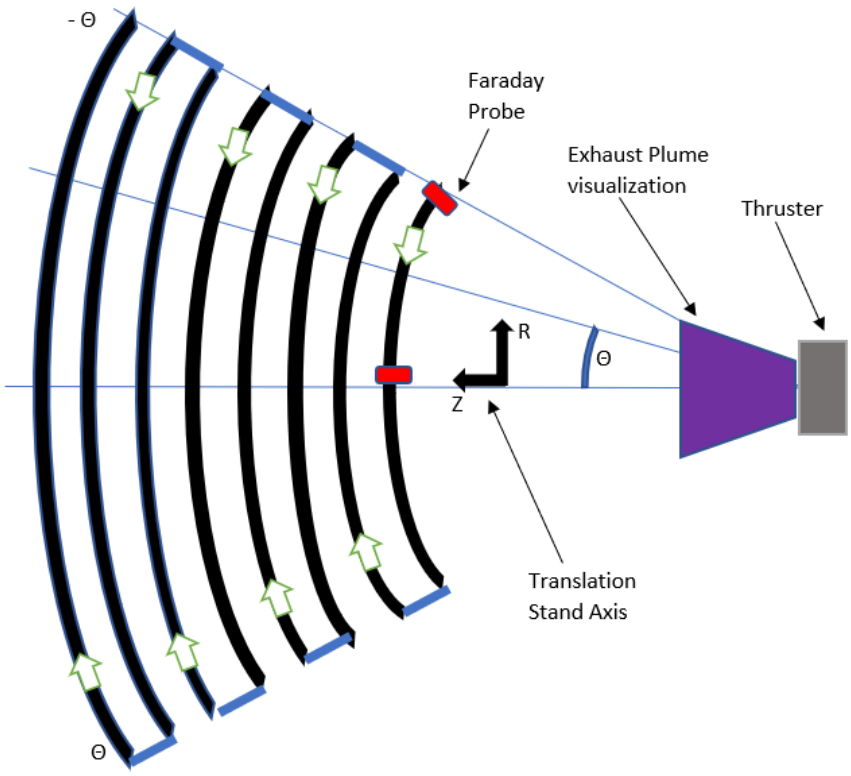

Figure 23: Faraday Probe sweep schematic

The data gathered from the probe sweep was used to create a plot of the current density of the exhaust plume. This plot was interpolated to find the half power angle to characterize the plume divergence. If the plot could not be interpolated due to restrictions in data gathering, i.e. the physical setup not allowing a wide enough plume sweep, the data was extrapolated using a gaussian/normal distribution fit curve to find the half power angle. The test was also run with the thruster situated in a vertical position, i.e. linear channel along the standard z-axis as opposed to the x y plane. An example of the plot from the data gathered in this research can be seen in figure 24 with the separate lines indicating the sweeps at differing radiuses.

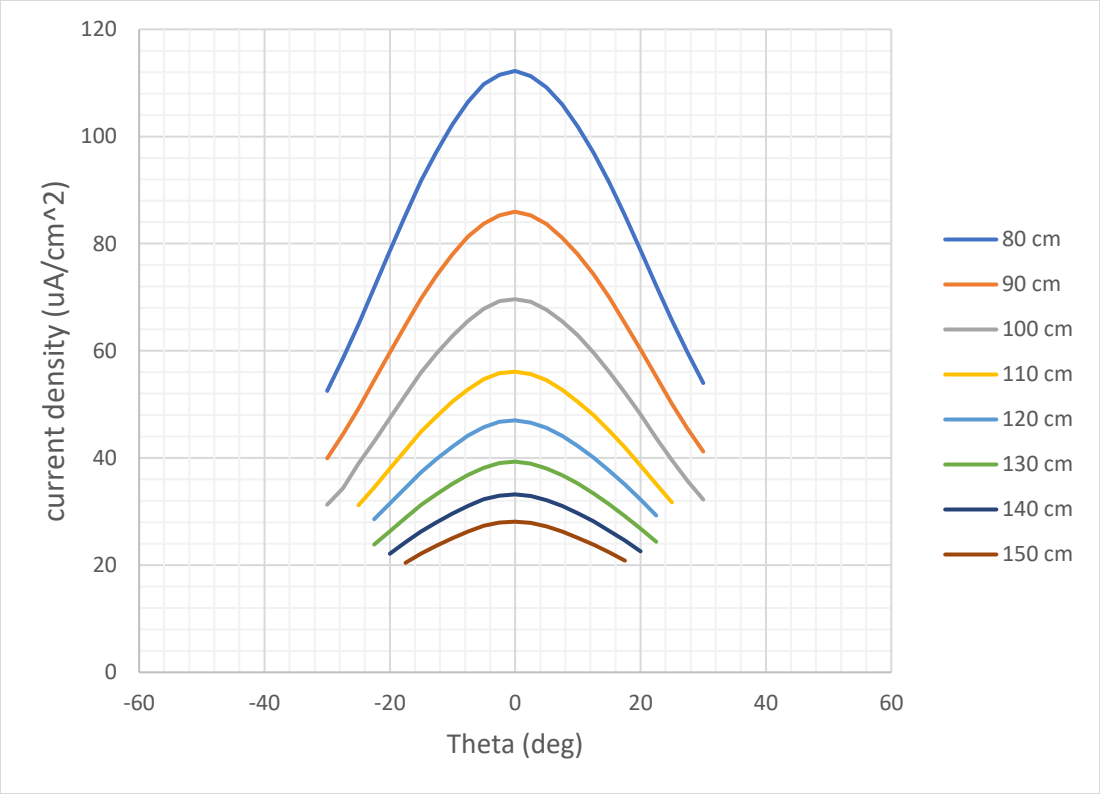

Figure 24: Example Faraday probe sweep plot

Chapter Summary

In this chapter, the planned experimental set-up and methodology for data post processing and analysis were discussed. However, certain aspects of the experiment were unable to be achieved due to equipment and time constraints, which will be discussed in the next chapter. Had all the experiments worked, this research would have provided time correlated data outputs from the oscilloscope, high-speed camera, and the emissive probe. Nonetheless, the experimental set-ups did provide the follow outputs: high-speed video of the plasma in the channel subsequently converted to a projected channel plot vs time, high-speed video of the instabilities of the plasma, and plume divergence data of the thruster emissions along two axes. Further data analysis and comparisons between the pseudo linear and cylindrical will be discussed in the ensuing chapters.

IV. Results and Analysis

Chapter Overview

In this chapter, the issues over the course of the experiment will be discussed, as well as summarizing and analyzing the data collected, and things discovered about the thruster will be mentioned. The high-speed camera data which is broken down into the projection plots will be discussed. In addition to the data collected from the Faraday for the thruster in both orientations will be discussed.

Experimental Delays and Issues with Equipment

Over the course of this research, several issues arose which hindered the ability to gather data either due to time or malfunction. First, data collection was significantly delayed due to a planned chamber extension, which occurred later in the year than expected. After the chamber was put back together with the extension secured, another delay arose due to the chamber not achieving operational pressures. This was troubleshot and resolved by ensuring all cabling was reconnected, and setting new changeover pressures between the pumps. As a result, this left little time to get some of the intended data sets. This also adversely affected troubleshooting of many of the measurement techniques, since they require the chamber to be pressurized to collect data and identify faults.

During thruster operations, other problems arose with the measurement equipment. The Faraday probe measurements were problematic in two aspects of data collection. First the probe's connection with the outside equipment required patching to ensure a good electrical connection for accurate data instead of only reading noise in the environment. Second, the translation stand would stop working after being in the vacuum

for a couple of hours. As a result, fewer variations in the data sets were able to be collected, i.e. varying thruster power settings. Limiting the data collected to one power setting to be analyzed.

The oscilloscope used for triggering the camera and probe, and reading the discharge output worked for both of those cases. However, it did not record data for the operator to analyze, probably due to an internal issue, any data acquired required an exterior note or picture from a camera to record the output. Also, during the operation of the emissive probe, it often burns out the filament resulting in its frequent replacement at atmospheric pressure. As a result of the aforementioned delays and the high sensitivity of the emissive probe, data collection was unable to be performed due to time constraints.

High-Speed Imaging

During thruster operation and after the thruster had been run at steady for an hour, as prescribed by the operation manual, data was collected on the Hall thruster's visible plasma emissions. The high-speed camera recorded the outputs collected on the range of 250,000 frames per second to 1,000,000 frames per second. However the camera only allows 102 frames to be processed consecutively at a time. These data sets were post processed (unwrapped) by the Matlab® script outlined in Appendix C, additional projection plots are in Appendix A.

Breathing Mode

By varying the thruster inputs to the discharge voltage and the current applied to the electromagnets, instability modes were able to be induced. From the input settings listed in Table 1, a breathing mode was able to be generated on multiple occasions, as

detailed in figures 25 and 26. Plots are in arbitrary scaling, from black to white heat map which represents a low to high presence of excited ions.

Table 1: Breathing Mode Thruster Inputs

Setting	input value	actual value	units
Discharge voltage	143	143	volts
Discharge current		3.2	amps
Magnet voltage		1.9	volts
Magnet current	0.5	0.5	amps
Heater voltage		0	volts
Heater current	0	0	amps
Keeper voltage		39.7	volts
Keeper current	0.5	0.2	amps
Anode mass flow	12.85	12.85	sccm
Cathode mass flow	1.34	1.34	sccm

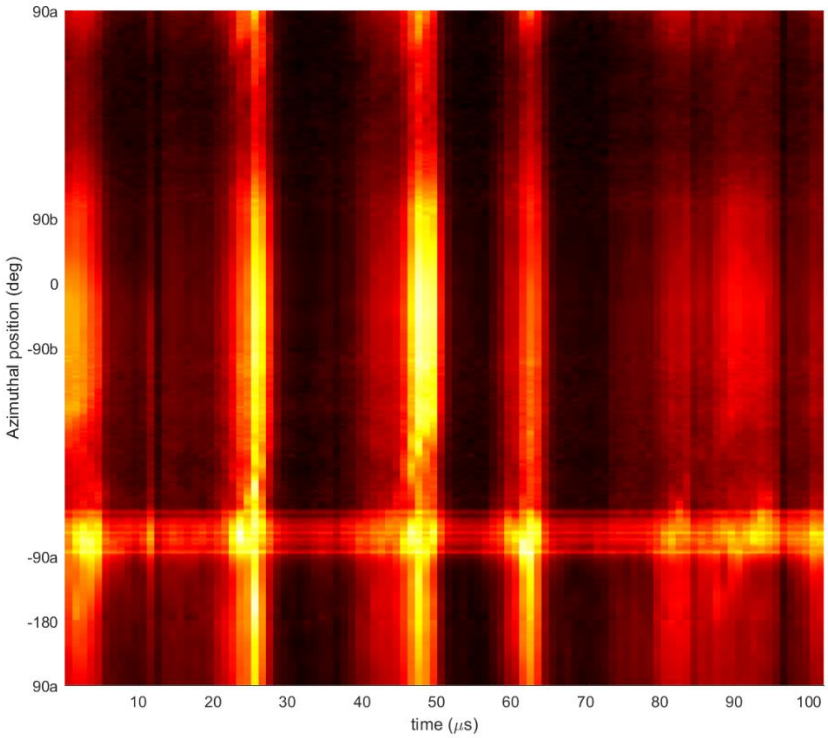

Figure 25: Breathing mode projected channel plot 1

From figure 25, it can be seen the local maxima for ionizations are achieved at t = 26, 48, and 63 µs. Analysis of these maxima would indicate the breathing mode frequency is on the scale of 40 to 60 kHz. Figure 26, represents a similar output with the thruster's settings within 1% of those used to produce the output seen in Figure 25.

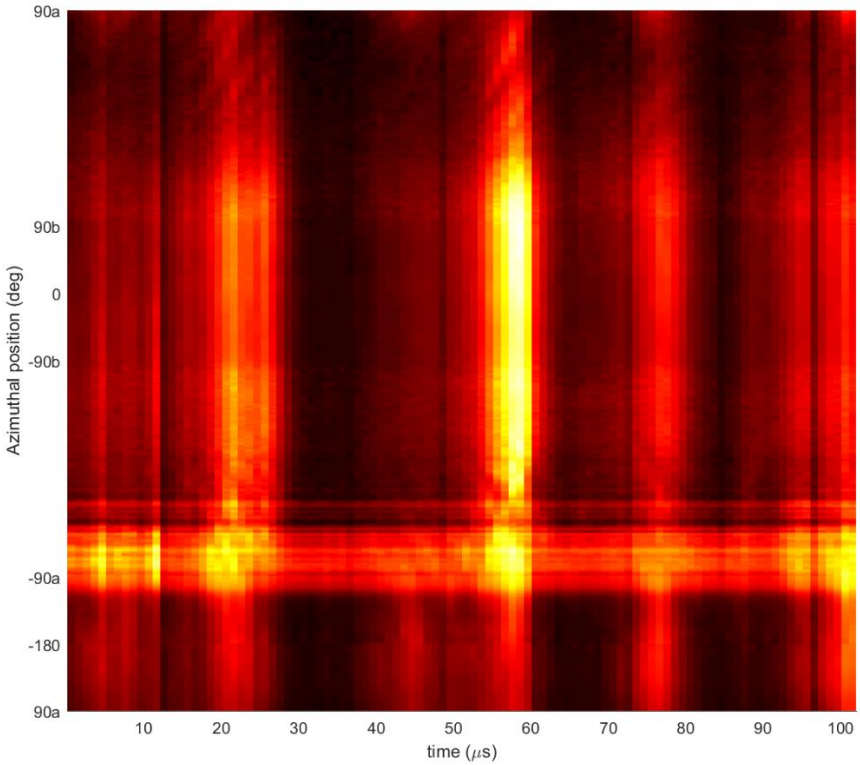

Figure 26: Breathing mode projected plot 2

The local maxima in figure 26 can be observed at t = 22, and 59 µs and faintly at 77 µs, the first to strong maxima indicate a breathing mode frequency at around 27 kHz. This is closer to the expected value indicated in earlier sections of between 15-22 kHz. However, these results may be skewed due to exposure times and the low time span required to illustrate breathing mode. With measurements hand recorded from the oscilloscope display, see appendix A., the frequency of the discharge currents peaks occurred at approximately 60 µs apart designating a breathing mode frequency at 16 kHz. When the

frame time was increased from 1 µs to 4 µs, allowing oscillation cycle, the visible emission data more accurately portrayed the thruster output data, as seen in figure 27.

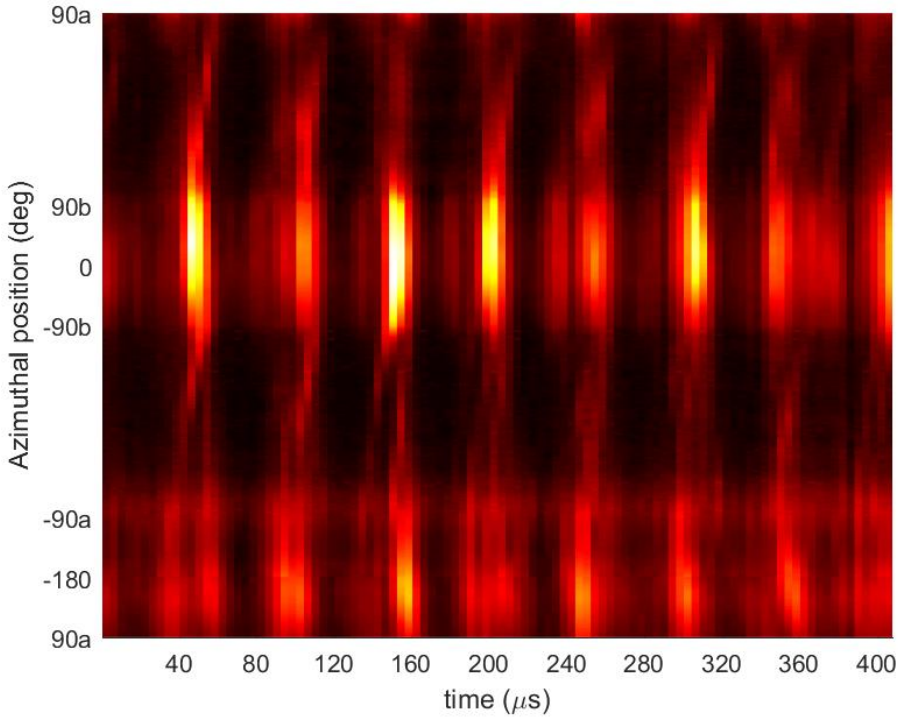

Figure 27: Breathing mode projected plot 3 slower data rate

From Figure 27, the average time between local maxima is approximately 57 µs, which puts the breathing mode frequency at around 17.5 kHz. This is in the range of what is expected and very similar to the data from the oscilloscope, which measures the discharge current of the thruster. However, during this breathing mode there appeared to be more activity in the turns, between 90a & -90a, and -90b & 90a, while the linear portions more accurately portrayed the oscillation in ionization. In the turns the intensity is consistently greater than the linear portions, but they peak at the same instances.

Due to the geometry of the pseudo linear thruster, the output of the breathing mode intensity oscillations is not as consistent as the cylindrical design. In typical cylindrical Hall thruster designs, the Hall current can move around the channel at a

constant speed and for differing designs this may not be the case. This is possibly due to compacted magnetic field lines in the turns as opposed to the linear segments and is further illustrated in the next section. However, when the sampling frequency is lower as in Figure 27 to allow complete cycles, the accuracy to perceived breathing mode oscillations [6] is increased.

Quasi-spoke Modes

In order to visualize what a spoke typically looks like in Hall thruster emissions, figure 28 provides an examination of a spoke, outlined by the green line, from previous research [23].

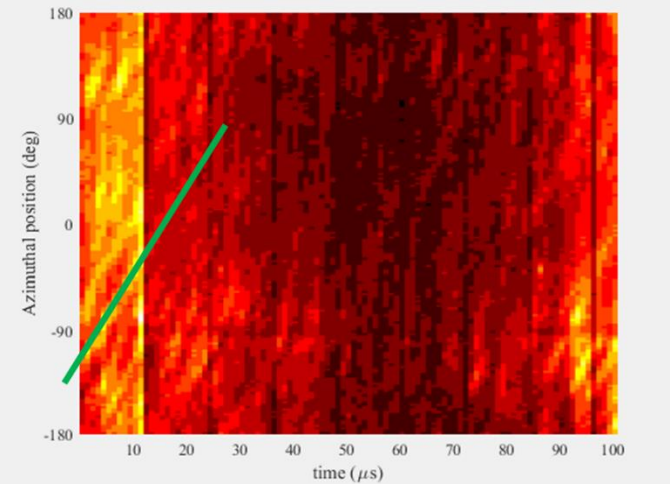

Figure 28: Unrolled spoke cylindrical Hall thruster [23]

As illustrated by the figure 28, the spoke moves in a linear fashion on the projection plot which translates to a constant speed around the channel. Spoke modes have been noticed in multiple manners in cylindrical thrusters, whether they are similar to figure 28 in that there are multiple spokes moving around the channel at a constant rate or a singular spoke moving around the channel. On the other hand, with the pseudo linear design the

thruster in present research was unable to generate a spoke that moves at a constant speed around the channel. mode.

Nonetheless, the pseudo linear hall thruster was able to generate spokes in select parts of the channel and particularly a quasi-spoke mode, in which the spoke would travel at varying rates around the channel, as depicted in figure 29. These varying rates of spokes have also been overserved in cylindrical designs [27].

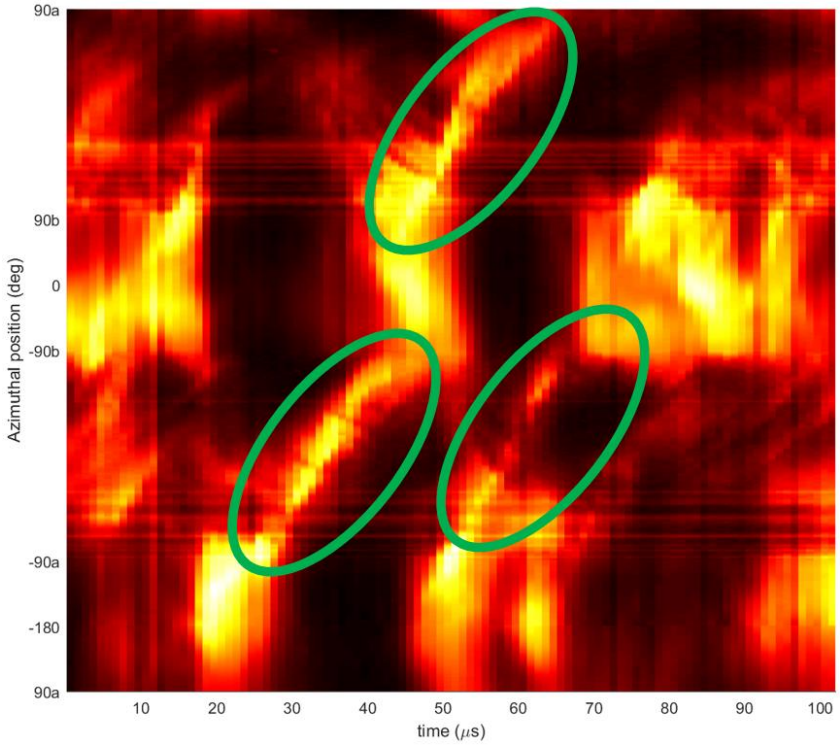

Figure 29: Quasi-spoke mode projection plot 1

As shown in figure 29, these spokes are identified by the green ovals, for the most part they assume a nearly linear path during the straights of the thruster channel. However, when in the corners they tend to ionize the entire region at once and leave on the next straight almost instantaneously. This behavior is uncharacteristic for a Hall thruster, since preferably there would be an equal number of excited ions in all regions of the channel. This is possibly due to the design of the thruster, with the gradients in the magnet field

varying around the channel. Subsequently, this instantaneous translation of the spoke around the whole corner is probably traceable to two things. First, the recessed center pole of the cavity allows for interaction between the opposite sides of the channel. Second, the actual geometry of the magnetic field is not consistent around the entire channel. Consequently, the Hall current may be taking a shortcut around the corner at the center of the channel where the magnetic field lines are more compacted. However, these characteristics are not understood enough to make a scientific explanation of what is going on with the flow of the plasma around the channel.

Furthermore, when the spokes were traveling along the straights of the channel, they would often decrease in intensity as they approached the other corner. Typically, the peak intensity of the spoke, ionization, would preferably remain somewhat constant as it moved around the channel. Since it would show that the same electron cloud region is moving around the channel at a consistent pace. As illustrated in figure 30, the intensity of the slice connecting the corners decreases over time, the reason for this is unknown.

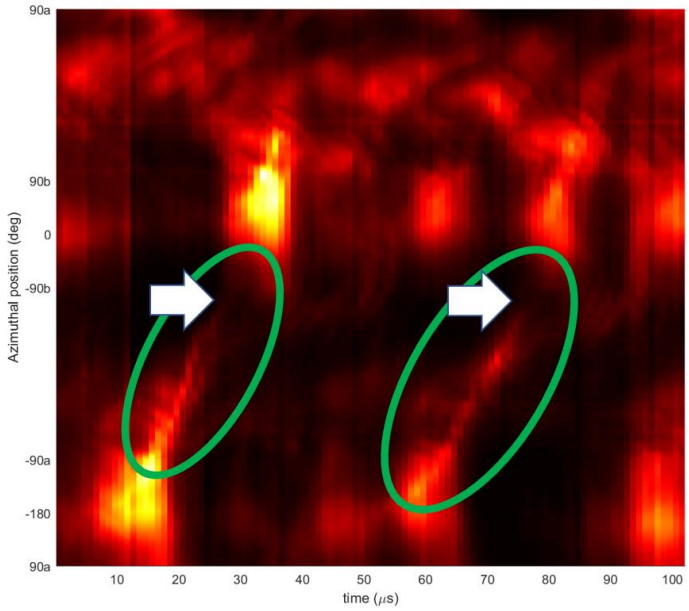

Figure 30: Spoke intensity diminution

Moreover, throughout the course of creating and analyzing these projection plots, it can be determined most of the ionization activity seen through visible emissions take place in the corners of the thruster channel, as in figure 31.

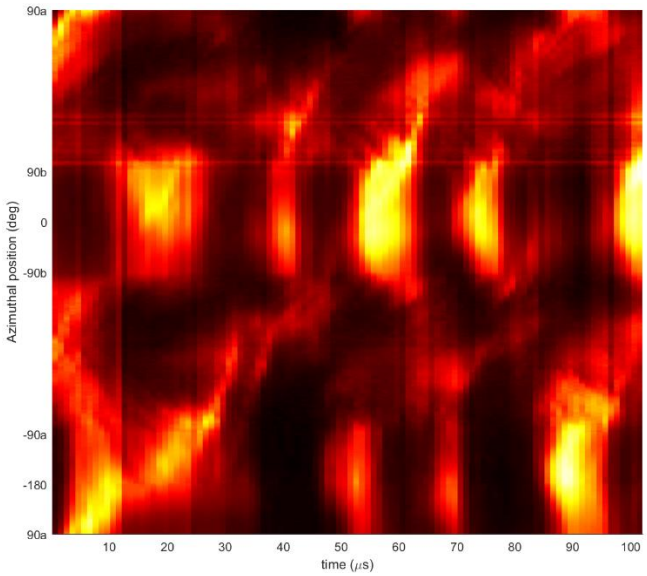

Figure 31: Pseudo linear projection plot 6

In conclusion, when examining the visible emissions with other designs, there are some similarities. Most importantly, the ionization or cloud of electrons are moving in the $\vec{E} \times \vec{B}$ field direction. This is in agreement with research done by others, Janes and Lowder, Sekerak, Cunningham, and Liu [7, 8, 9, 27]. From observations done in previous research of cylindrical Hall thrusters there was no preferential origination location of these spokes. However, since most activity took place in the corners, spoke generation appeared to take place there as well but is not verifiable in this research. Nonetheless, similar to the cylindrical thrusters, spokes did appear to cluster in spots [7]. In all, even though the manner in which the plasma moves throughout the pseudo linear thruster channel is not well understood, there remain some commonalities with the cylindrical design.

Faraday Probe

During steady thruster operations, three differing tests were run with the Faraday probe. First, the probe was mounted on the probe translation stand and the thruster was mounted horizontally on the other translation stand. Given the limitations of the stand and lengths of electrical wiring the probe was run from an elevated position (7 cm) above the thruster centerline and at a minimum radius of 75 cm. With the probe mounted in this elevated position, ion collection may have been obscured due to the line of sight between the aperture and thruster cavity. As a result, the data gathered from this test was not as accurate as the following tests but gave a representation of how the current density varies with radius and position in plume. The data associated with this test can be found in Appendix B. Following this test, the stand was adjusted to move the probe mounting position to be centerline with the thruster, as depicted in figure 32 below.

All data for the Faraday probe was collected with the Hall thruster set to and operating at the same inputs. This table of inputs and measurement values can be found in Appendix B. Due to limitations for the translation stand, data was unable to be collected for the entire inputted arc. As a result, the data outputs for these unreachable locations read as zero, but were negated because the probe was not gathering data.

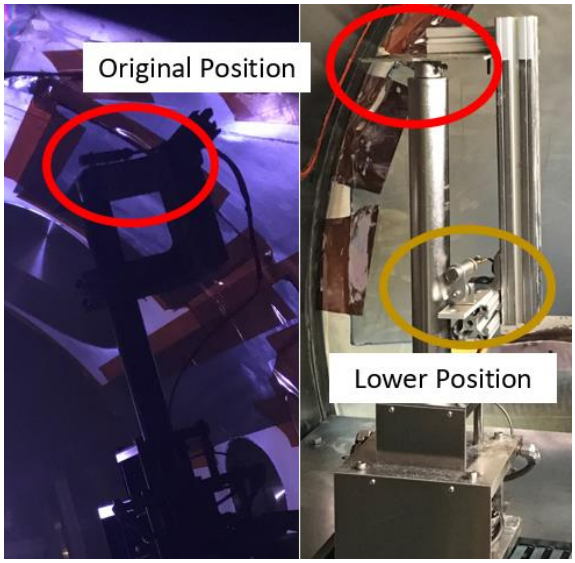

Figure 32: Faraday probe mounting

Probe Level with Horizontally Mounted Thruster

With the probe mounted level to the center of the Hall thruster discharge cavity, the probe swept out an arc like path. With a 120 degree arc broken down into 2.5-degree increments, and radial distance from 80 cm to 150 cm in 10 cm increments. Ten separate sweeps were done with the same settings to generate an average. The data was analyzed as mentioned in previous sections and plotted with respect to angle and radius, figure 33 shows the results.

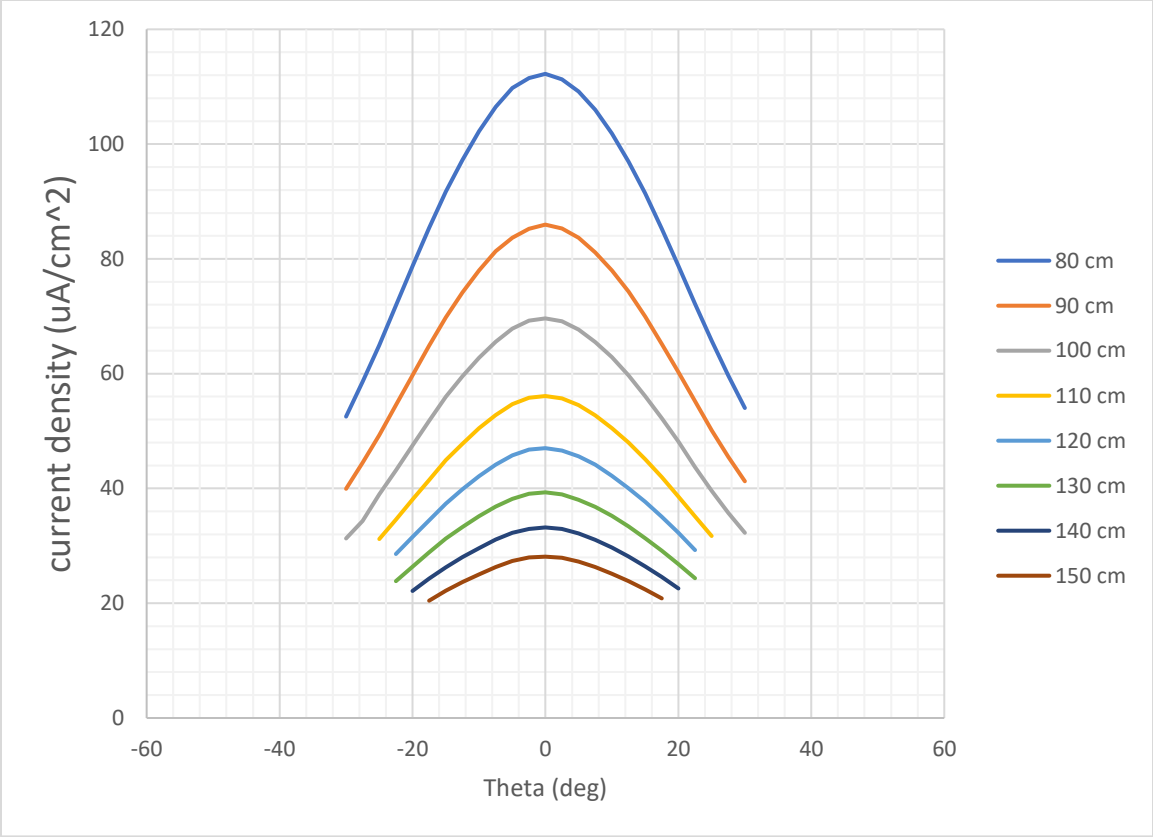

Figure 33: Faraday plot horizontal thruster

Again, the sudden termination in the radial data lines is due to the inability of the probe to reach the desired collection location. As expected the plot shows with an increase in radius the current density dramatically decreases. In addition, the plot represents a Gaussian distribution similar to the results established by Bui [26]. One important feature that can be noted from this data set is the half-power angle or full width at half maximum (FWHM). This value gives insight into the plume divergence and generates critical "keep out" regions for other equipment to avoid exhaust bombardment. The FWHM is found by identifying the intercepts along the same curve at half the peak value and calculating the difference between those angles. For the horizontal plane the FWHM is 57.6 degrees, diverging roughly 28.8 degrees off centerline in each direction.

Probe Level with Vertically Mounted Thruster

All the same procedures and techniques are the same as the previous data collection above with the only variation being the orientation of the thrust rotating 90 degrees, as shown in figure 34 with the results in figure 35.

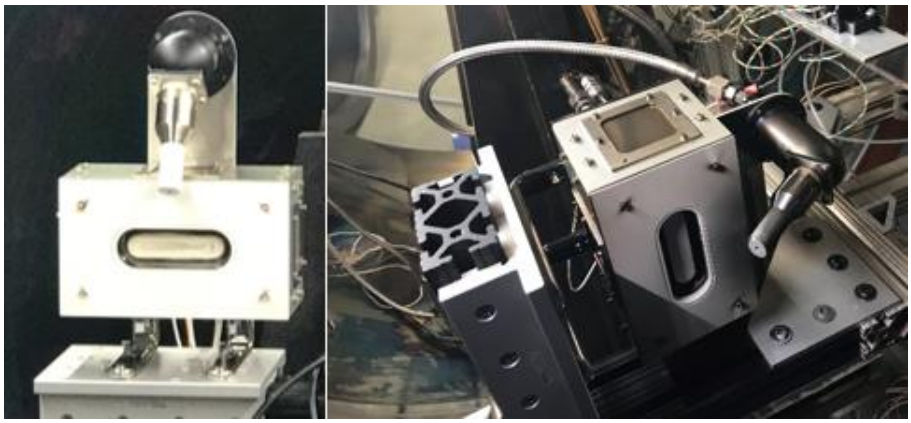

(a) Horizontal (b) Vertical

Figure 34: Thruster orientation

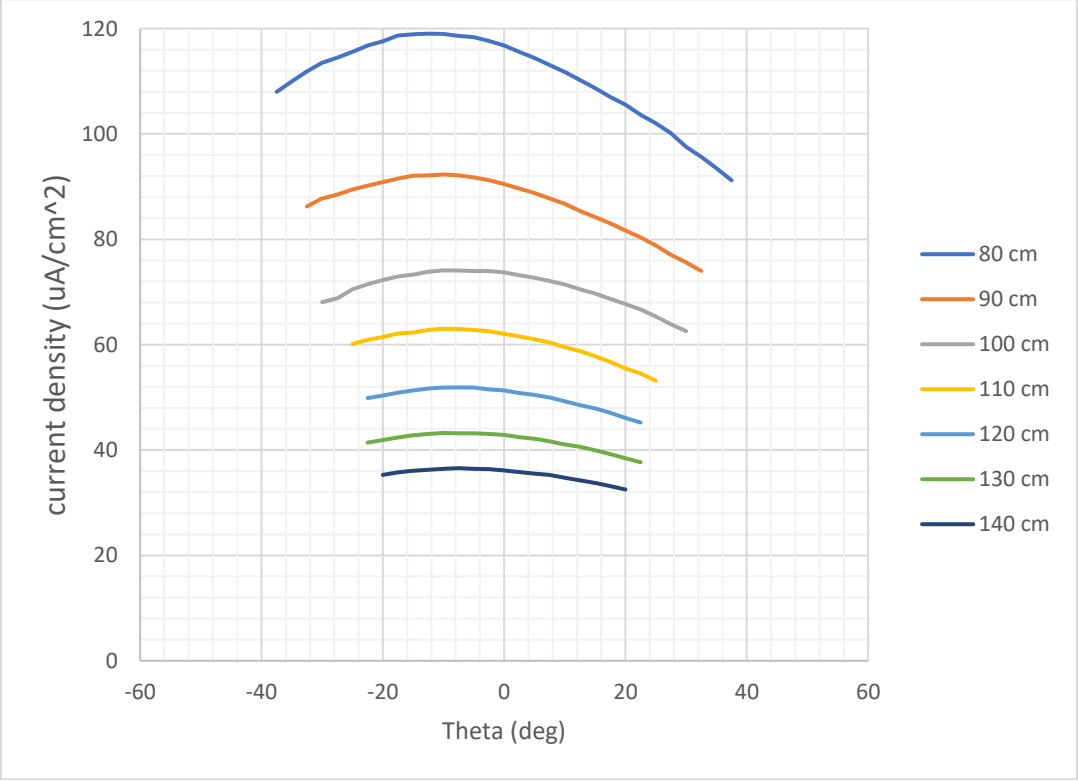

Figure 35: Faraday plot vertical thruster

Once again, the plot indicates as radius increases current density decreases and it represents part of the Gaussian distribution, as seen in Figure 36.

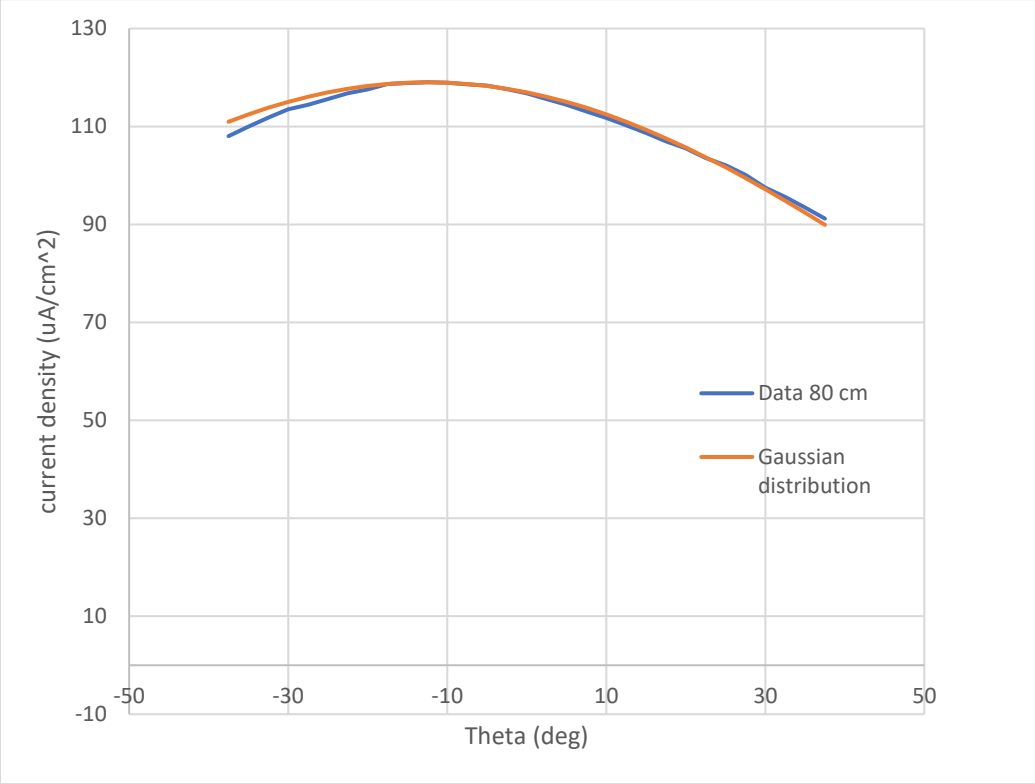

Figure 36: Gaussian Fit, Faraday Probe Vertical

However, the plot does not extend far enough to gather useful information about the plume divergence. In order to extrapolate on the data a Gaussian curve was matched to the curves, the magnitude of the created curve was adjusted for the representative center point magnitude of each curve. However, when selecting the best standard deviation for the curve, only one value was used for all seven data sets. The best option for standard deviation was determined by gathering the sum of the residuals squared of each plot, only using the data for angles measured. Once a local minimum in the sum of residuals squared was reached, the standard deviation was set and Gaussian distribution plots were developed, as shown in figure 37.

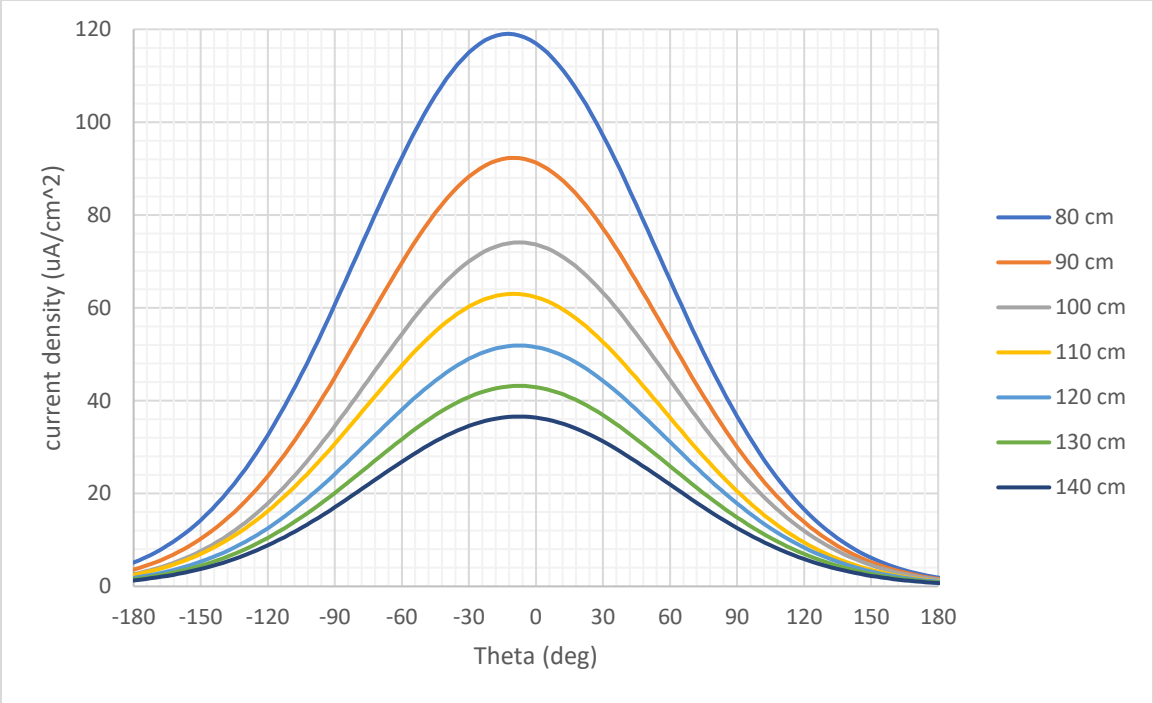

Figure 36: Faraday vertical estimated Gaussian distribution plot

From the Gaussian distribution data, the plume divergence data desired is obtainable; for the vertical setup the FWHM is 156.5 degrees, diverging roughly 78.25 degree off centerline in each direction. Another featured noticed as a result of this experiment is that offset in center line due to cathode influences. Noticeable from figure 35, the peak of the curves is not along the centerline of zero as the test is setup, and the peak center varies with radius. From the initial radius of 80 cm and up the peak offset in degrees is -12.5, -10, -7.5, -10, -7.5, -7.5, -7.5; with the greatest deviation being the closest measurements, which is where the cathode would be expected to have the greatest influence on the plume.

Thruster Anomalies

Before addressing the anomalies seen in the thruster output, the design of the thruster is important. As shown in figure 5, which displays a schematic of the thruster

designed and built by Busek in the late 1990s, it depicts an array of separate electromagnets surrounding the channel. This is a typical design used for Hall thrusters, as it is common in the cylindrical channel design. The proposed and actual schematic for the Hall thruster used in this experiment are illustrated in figure 38.

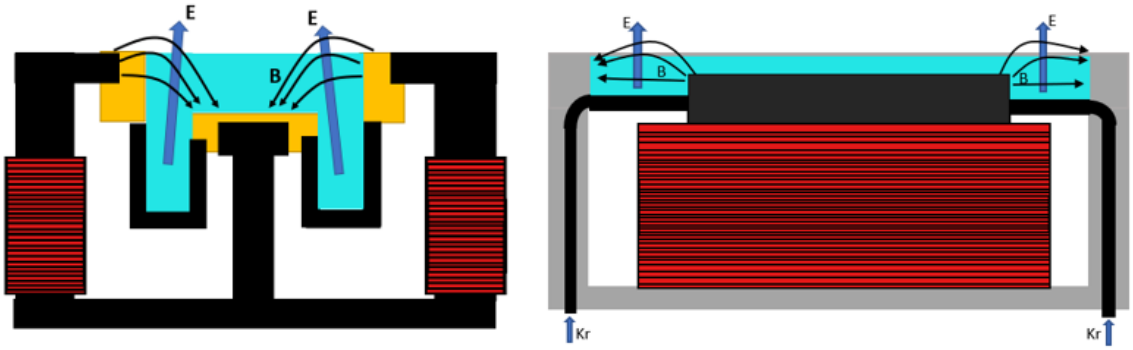

Figure 37: Pseudo linear design schematics: proposed (left), actual (right)

In the proposed schematic the location of the electromagnet is outside the channel, in the actual the electromagnet is along the center of the channel. Figure 39 shows the actual pseudo linear Hall thruster illustrated in the (right) schematic.

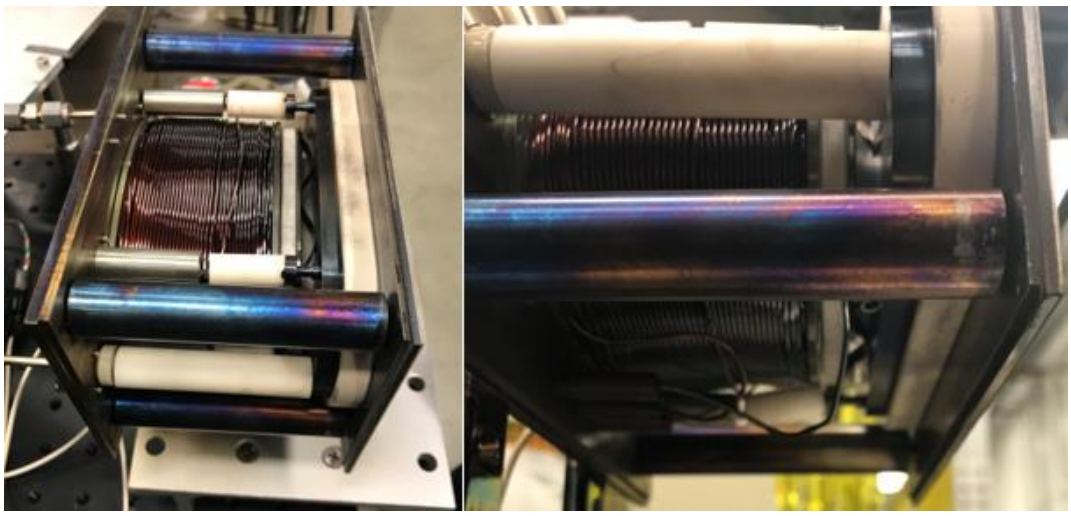

Figure 38: Thruster: view from top/right (left), bottom/right (right)

Hot spots

During thruster operations, visual irregularities, emissions other than Krypton, were spotted in the channel of the thruster, particularly in two distinct locations mirroring each other. These locations exist, if following the counter clockwise path, on the exit of the turn along the inside edge of the channel, as shown in figure 40, 41.

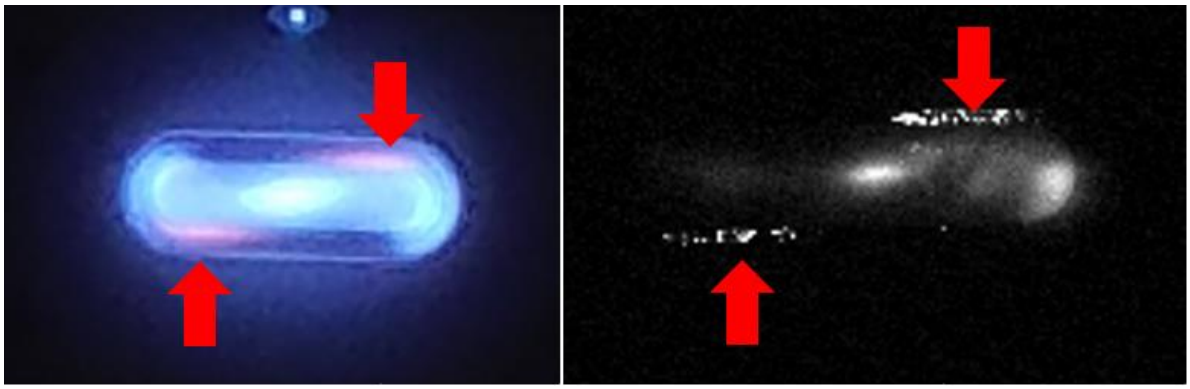

Figure 40: Visible discoloration on thruster channel

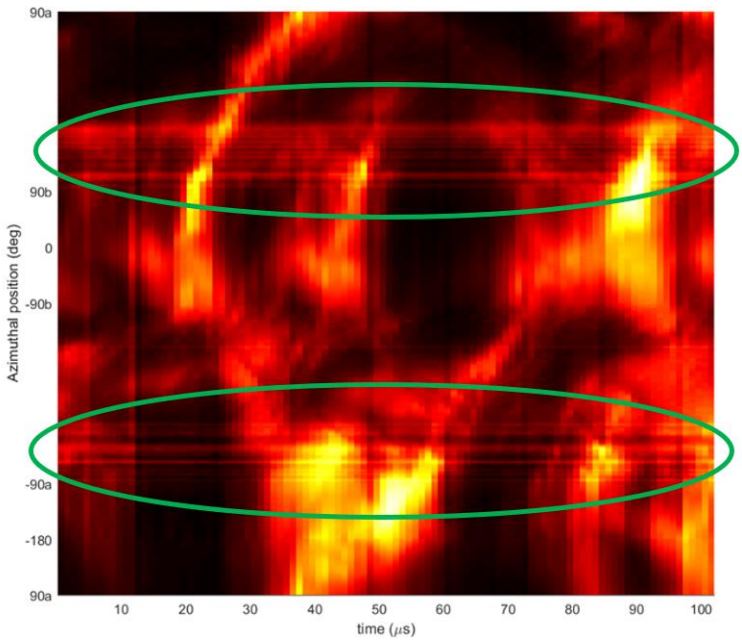

Figure 39: Visible discoloration in unwrapped images

Figure 40 depicts a normal camera image on the left and a high-speed image on the right. In both of these images it is noticeable the ambiguity exists in the corner exit locations.

Also, figure 41 indicates this phenomenon in the unwrap of high-speed camera data; where the irregularity remains at the corner exit locations and are thus represented as stripe, above -90a and 90b. Since this irregularity is consistently present, it sparked interest into what may be causing them and what type of photons they were emitting.

As a result, tests were run utilizing spectrometers; the first test utilized a spectrometer with a large field of view that was unable to distinguish the spot from the krypton ions in the plume. However, the second test utilized a Headwall A-Series Hyperspec VNIR imaging spectrometer. That uses a modified Offner design with a curved diffraction grating, and was equipped with a 0.8 Mpix camera, a 25 micron entrance slit, and 500 nm long-pass filter. The resultant data, figure 42 shows the graphical output of the data, the rows go vertical with the peak just above the inside of the channel wall, indicating a broadband emission. The temperature of these spots was estimated, by Dr. Hawks, at 2000 +/- 300 K.

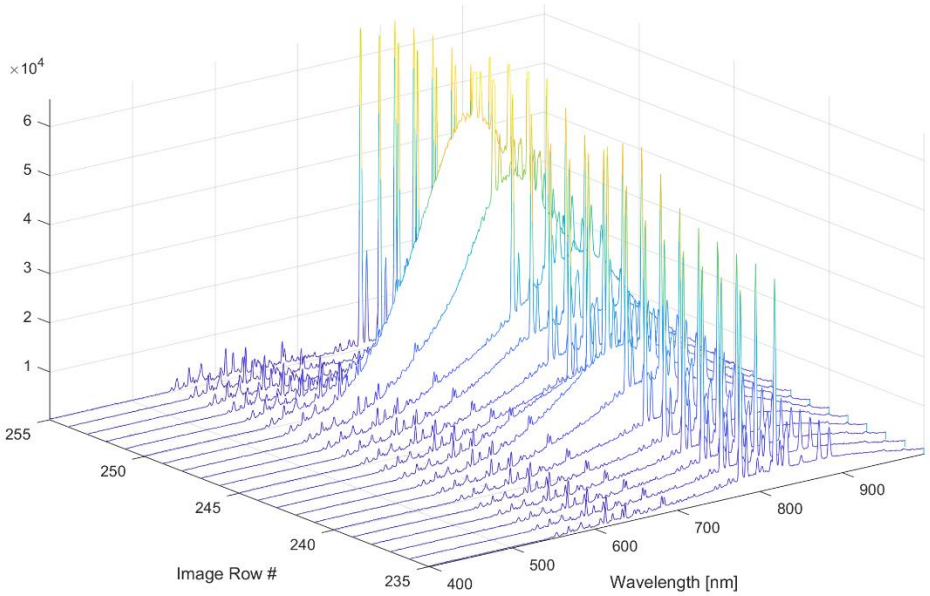

Figure 40: Spectrometer output for hot spot

At atmospheric conditions, the thruster was also visually inspected to determine if there had been any effects on the thruster as a result of these hot spots. Erosion of the channel insulator was noticed in the corner exits, as indicated in figure 43. Even though the erosion was minuscule at the present time, the continuation of erosion will negatively affect the lifespan of the thruster.

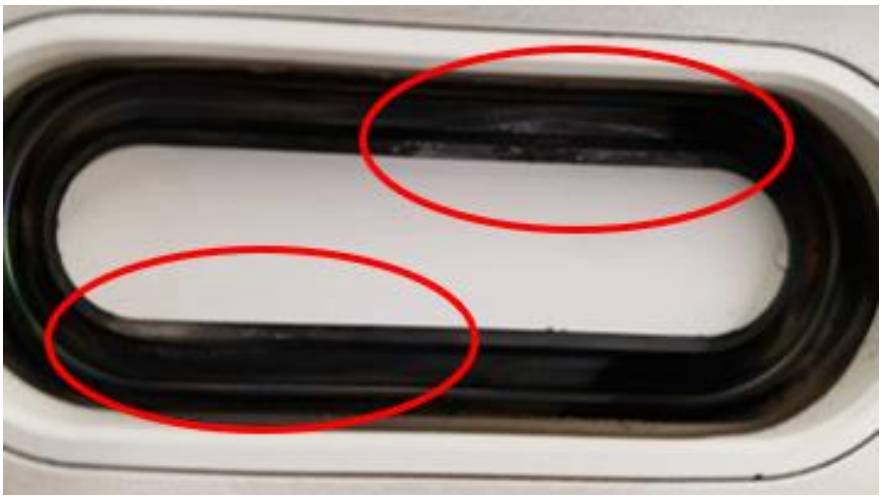

Figure 41: Visual Erosion on Channel

V. Conclusion & Recommendations

Conclusions of Research

The original objectives of this research were to measure plume current distribution, as well as high-rate time correlated measurement of plasma potential, discharge current, and visible emission from a pseudo-linear Hall thruster. However, as a biproduct of delays and equipment issues, some of the original objectives went unmet. On the other hand, the data gathered did produce some interesting observations about what was going on in the plasma. The high-speed camera data showed the oscillations of a breathing mode and its associated frequency. This frequency fell within the range of predicted values for Hall thruster plasma oscillations. Also, the thruster showed some signs of a spoke mode, but not a full generation of one as observed in cylindrical designs. Interestingly, the visual emissions indicated there is a lot of unexplained plasma tendencies occurring in the turns of the channel. The Faraday probe data demonstrated a Gaussian distribution and indicated differing plume divergences based on orientation. Most importantly, visual emissions and inspections showed there is erosion occurring during thruster operation, potentially having a large impact on thruster life span.

Significance of Research

Performed plume characterization measurements on a revolutionary pseudo linear Hall thruster. The potential advantages of this design are that it enables linear scaling of thrust and improved packaging for satellite integration. Also, the non-intrusive measurement plasma behavior with high-speed imagery within the channel of the pseudo linear Hall thruster, enriched understanding of the channel geometry effects on the plasma. As well as, the plume divergence characterization along two axes can be used to

create regions on the spacecraft near the thruster to be clear of unwanted exhaust bombardment. Finally, a key anomaly, potentially due to the design, was identified in the thruster operation that caused multiple local heating locations and erosion to the channel insulator. This anomaly can limit the potential life span of the thruster.

Recommendations

Since some of the research objectives went unmet due to equipment malfunctions, these problems can be alleviated before the start of future testing. Once, addressed these measurements can be performed and data collected.

For future research involving the pseudo linear Hall thruster, the use of intrusive probes might come in handy when trying to examine what is going on in the turns within the cavity. Nonetheless, just attempting to use differing probes at locations around the channel may generate a greater understanding into how the plasma moves about. Extension or replacement of the electrical wiring inside the chamber may be beneficial in taking future Faraday probe measurements at a closer range to generate distribution plots. Instead of extrapolating on a small set of data points. Additionally, one may affix the cathode along the other axis of the channel to gain insight on the effects it has on plasma behavior given the unique design of the thruster. Another consideration would be to improve the camera setup in order to achieve better resolution images.

Summary

The Busek 475 W pseudo linear Hall thruster tested in this research was successfully started and restarted with ease on multiple occasions. The thruster was able to run for hours without user input to modify settings. However, in order to start thruster operations, several obstacles concerning the chamber extension and pressurization had to

be overcome. Further testing is required to gather plasma potential data along with time correlated measurements. The use of a racetrack cavity proved to create interesting plasma behavior. It also, potentially caused the formation of hot spots on the channel resulting in erosion. The cavity design also generates differing plume divergences which may be beneficial in packaging considerations. This thruster design may require a bit of tweaking to generate desired or at least similar spoke behavior as observed in cylindrical designs.

Appendix A. Additional High-Speed Data

Oscilloscope

Oscilloscope readouts to verify breathing mode frequency

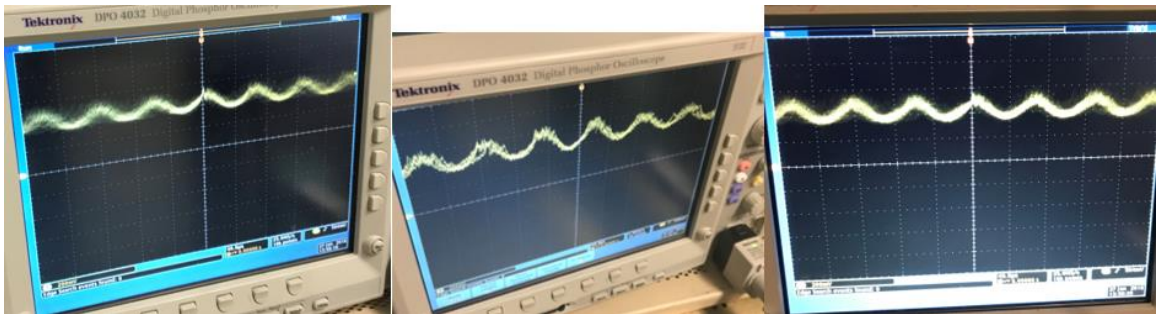

Figure 42: Oscilloscope output

Additional Projection Plots

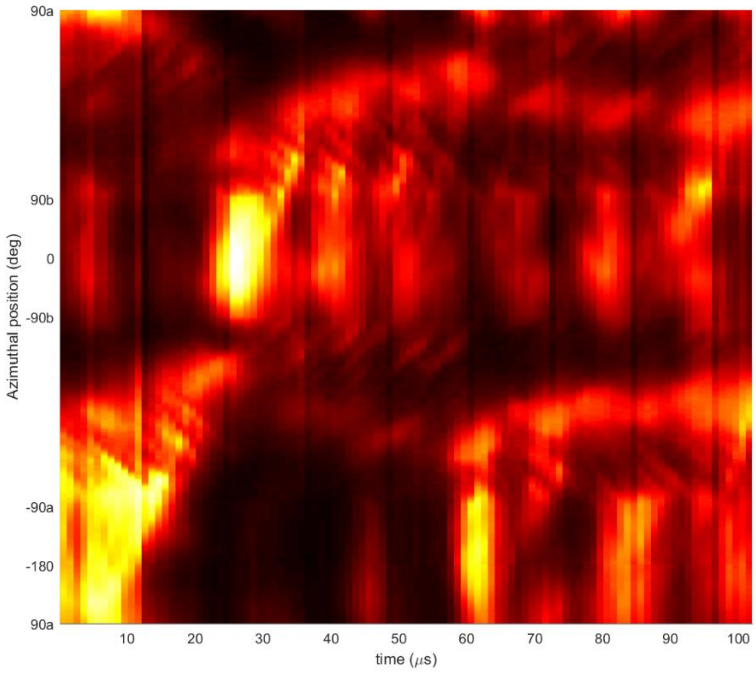

Figure 43: Pseudo linear projection plot 7

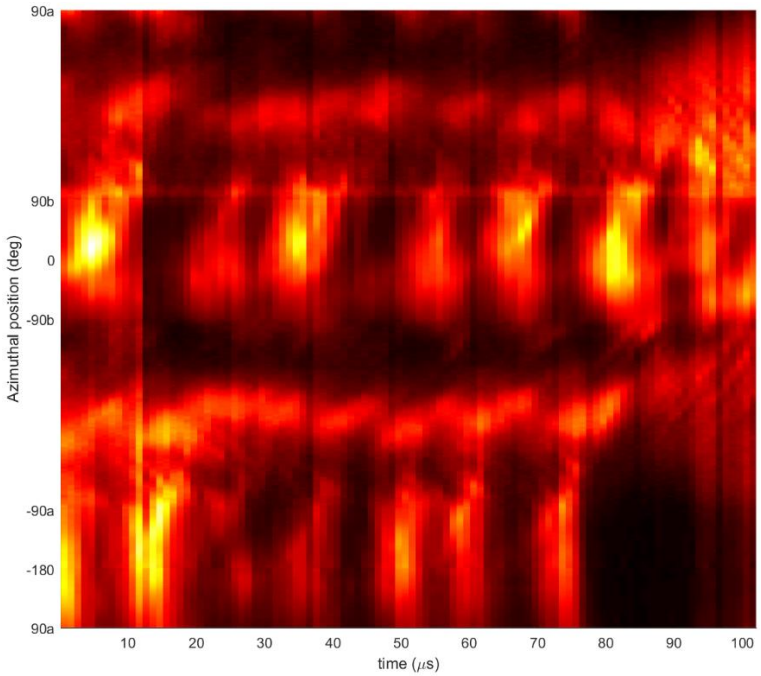

Figure 44: Pseudo linear projection plot 8

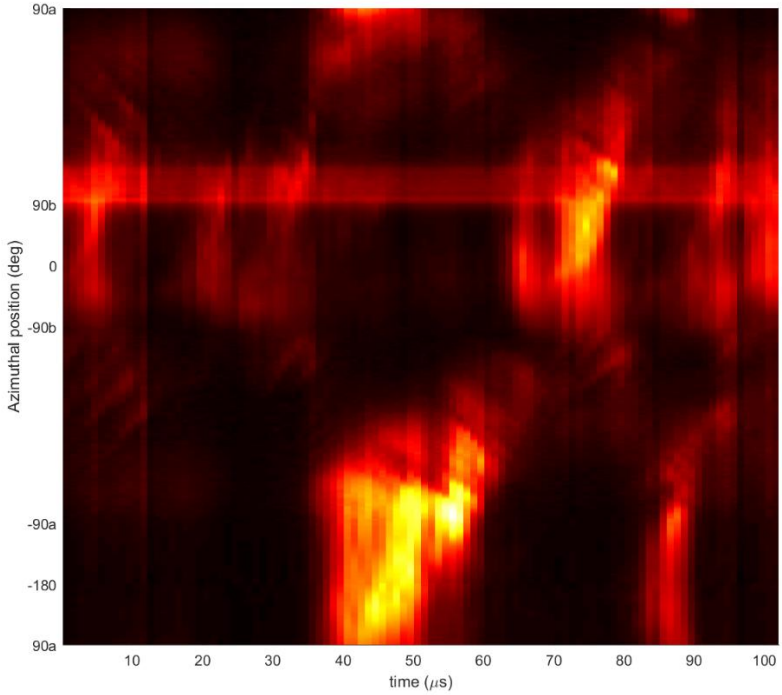

Figure 45: Pseudo linear projection plot 8

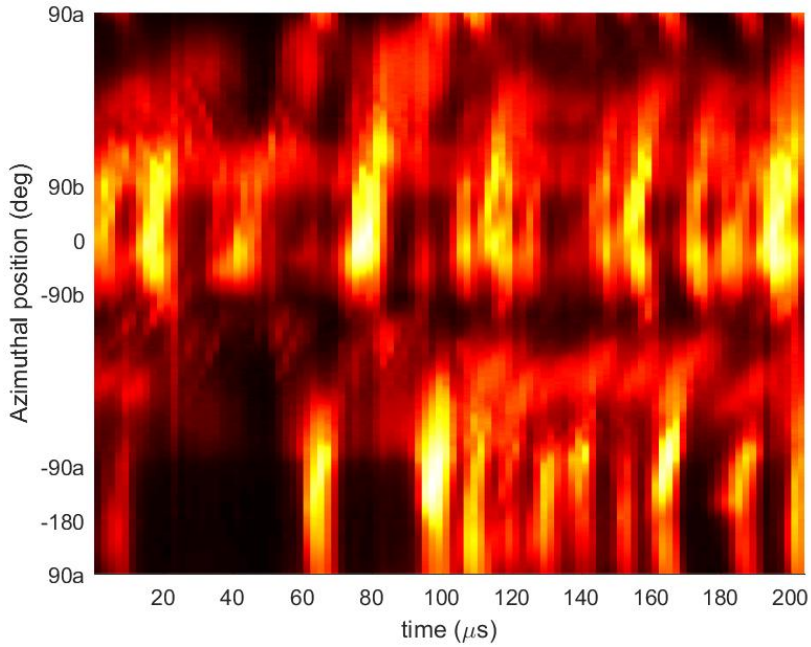

Figure 46: Pseudo linear projection plot 9

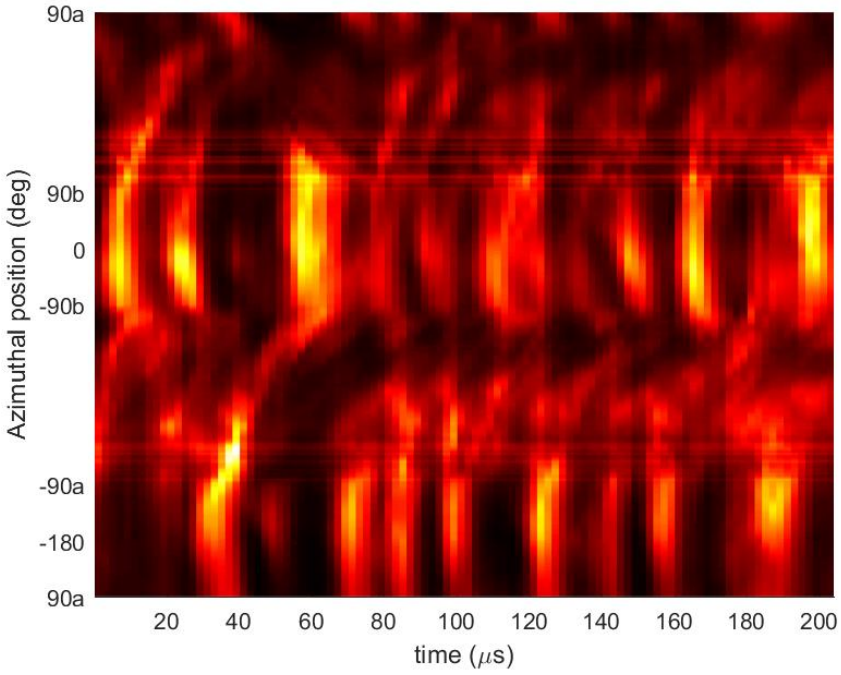

Figure 47: Pseudo linear projection plot 10

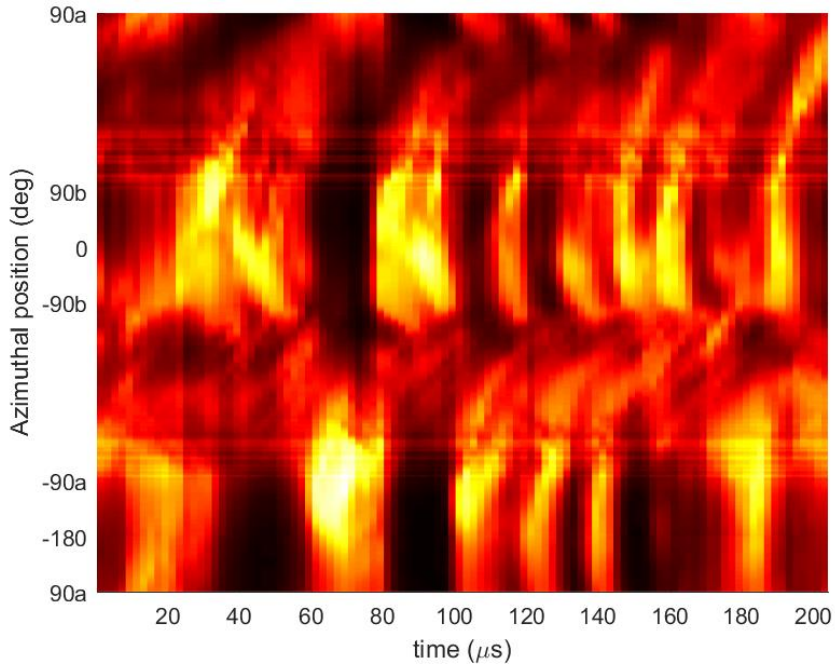

Figure 50: Pseudo linear projection plot 11

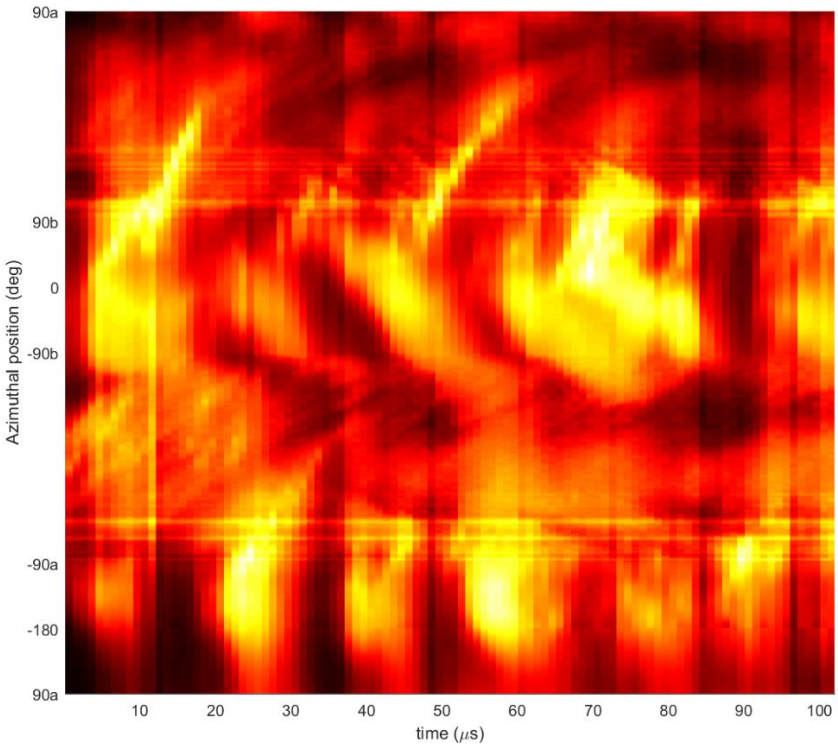

Figure 48: Pseudo linear projection plot 12

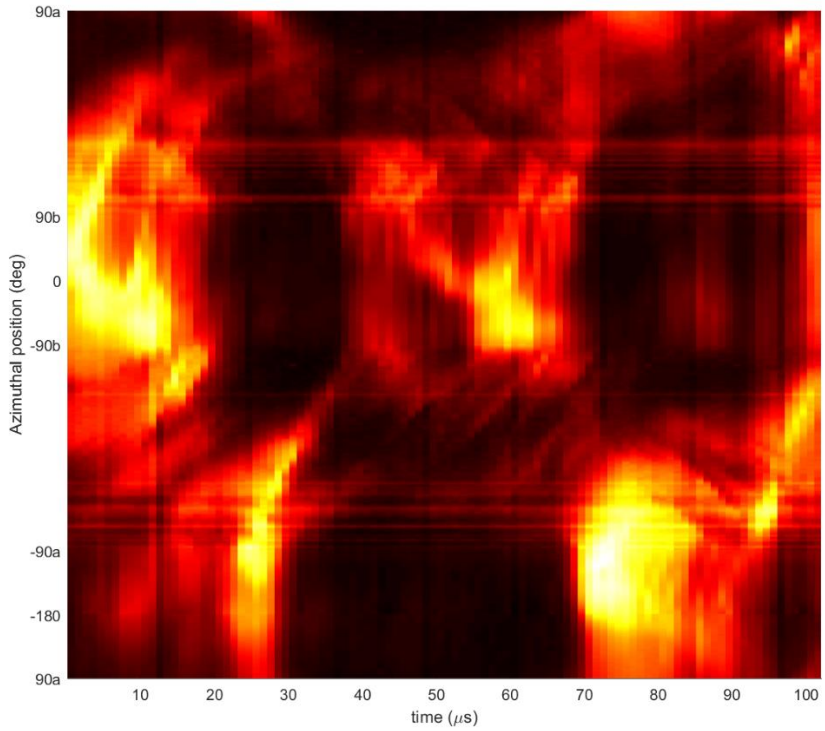

Figure 49: Pseudo linear projection plot 13

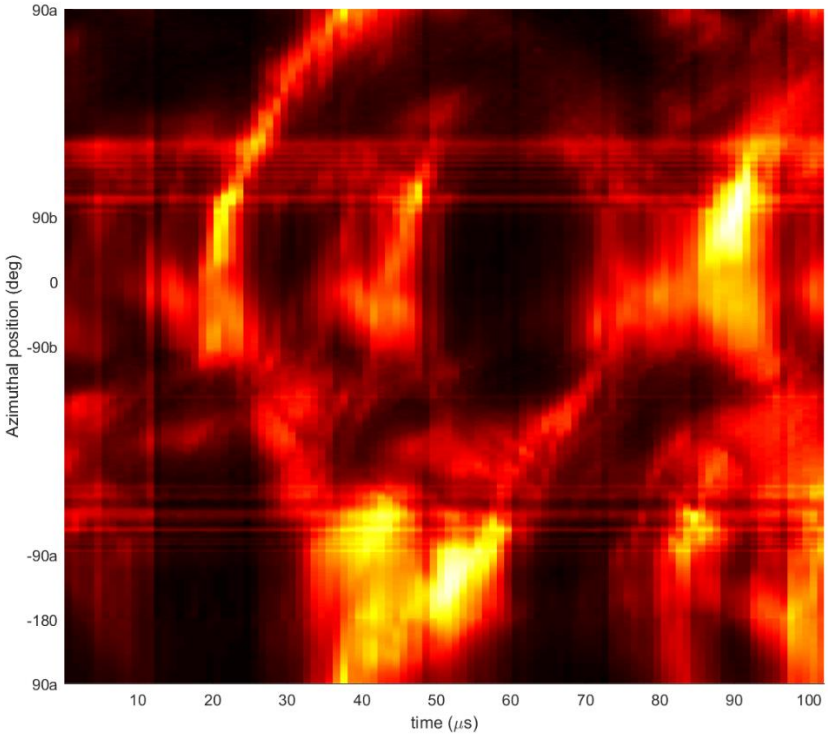

Figure 50: Pseudo linear projection plot 14

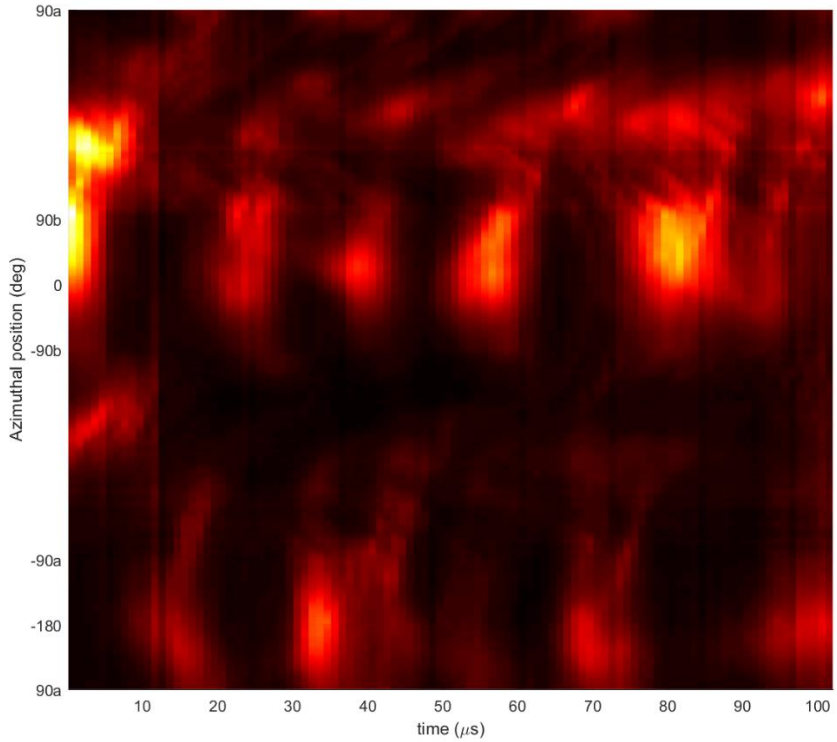

Figure 51: Pseudo linear projection plot 15

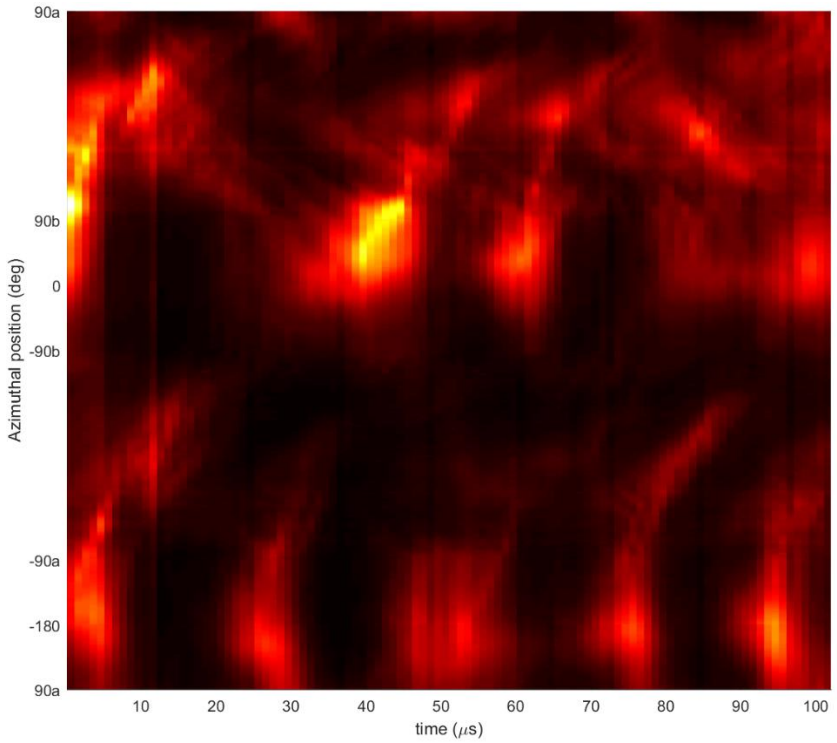

Figure 52: Pseudo linear projection plot 16

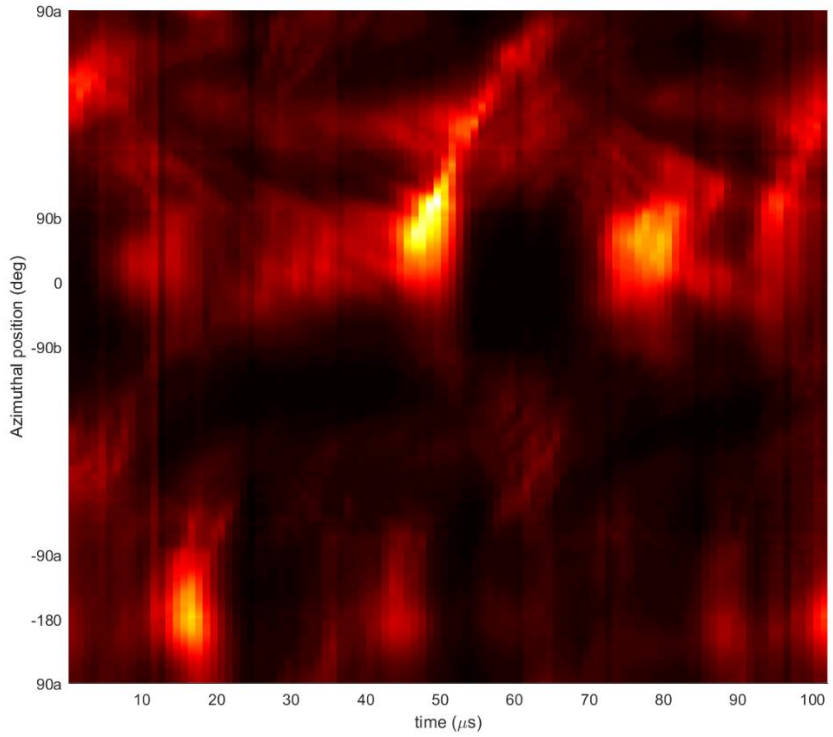

Figure 53: Pseudo linear projection plot 17

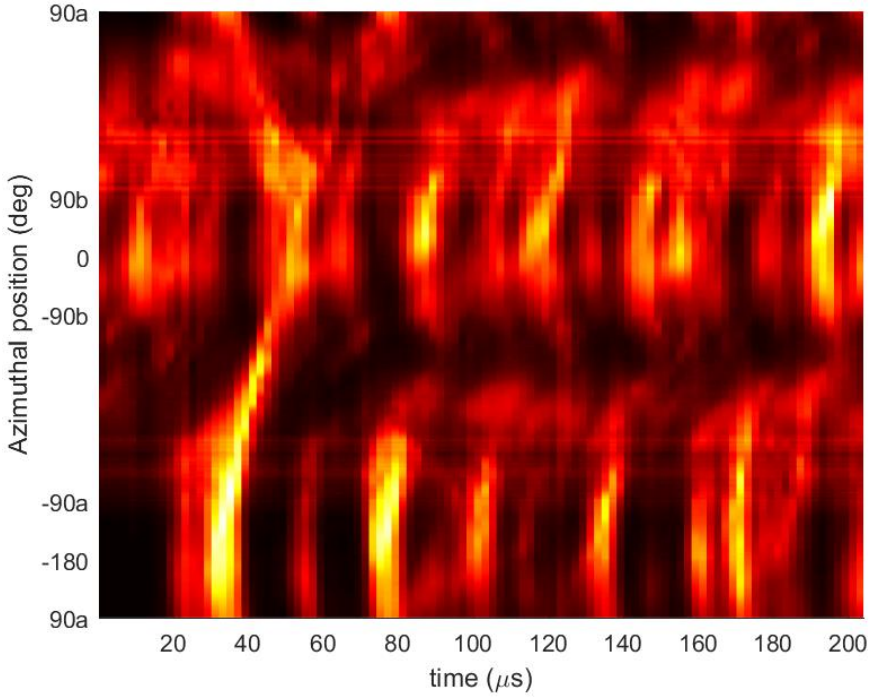

Figure 54: Pseudo linear projection plot 18

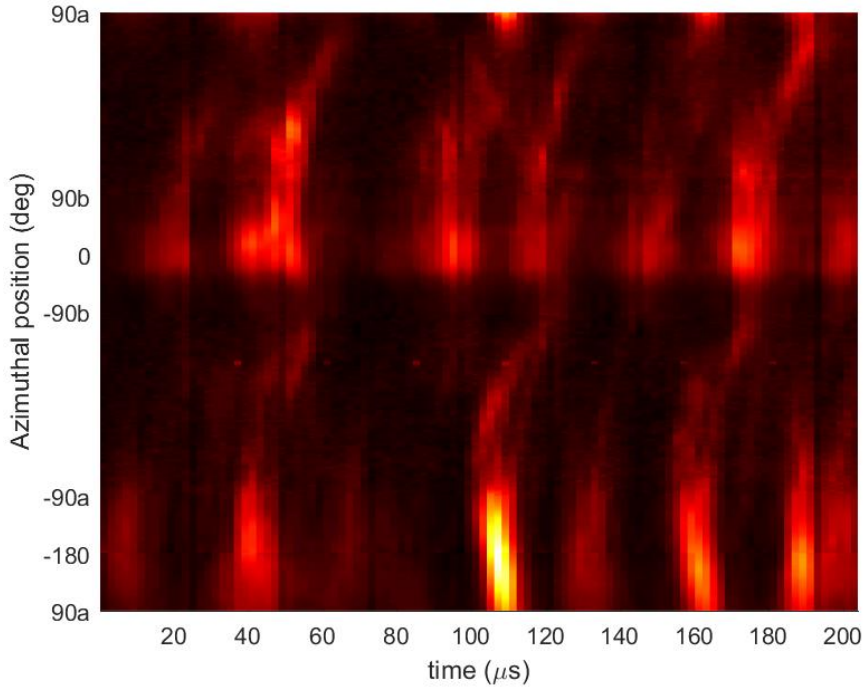

Figure 55: Pseudo linear projection plot 19

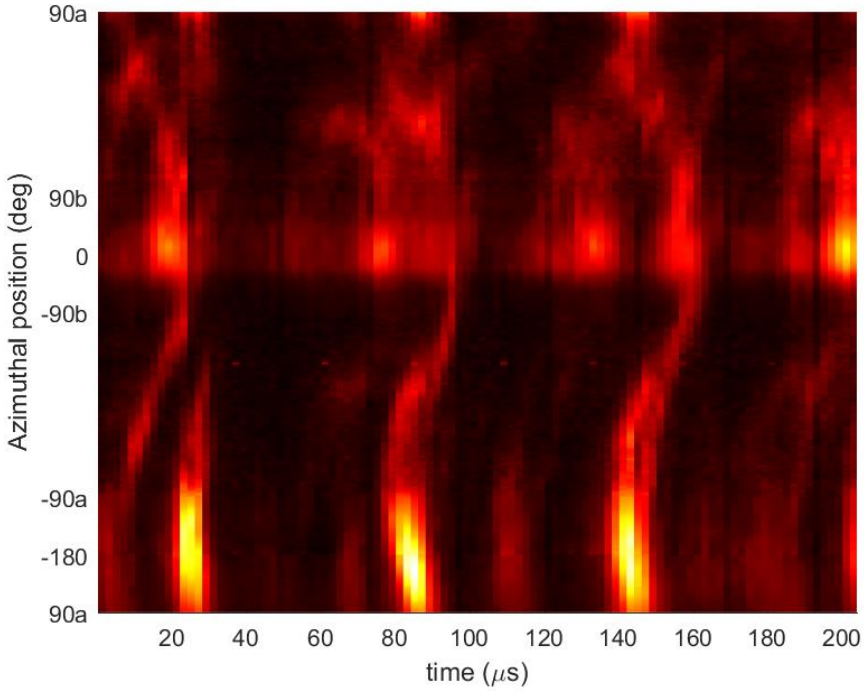

Figure 56: Pseudo linear projection plot 20

Appendix B. Faraday Data

Table 2: Thruster Settings Faraday Probe

Setting	input value	actual value	units
Discharge voltage	200	198	volts
Discharge current		1.6	amps
Magnet voltage		4.1	volts
Magnet current	1	1	amps
Heater voltage		0	volts
Heater current	0	0	amps
Keeper voltage		37.4	volts
Keeper current	0.5	0.2	amps
Anode mass flow	13.35	13.35	sccm
Cathode mass flow	1.65	1.65	sccm

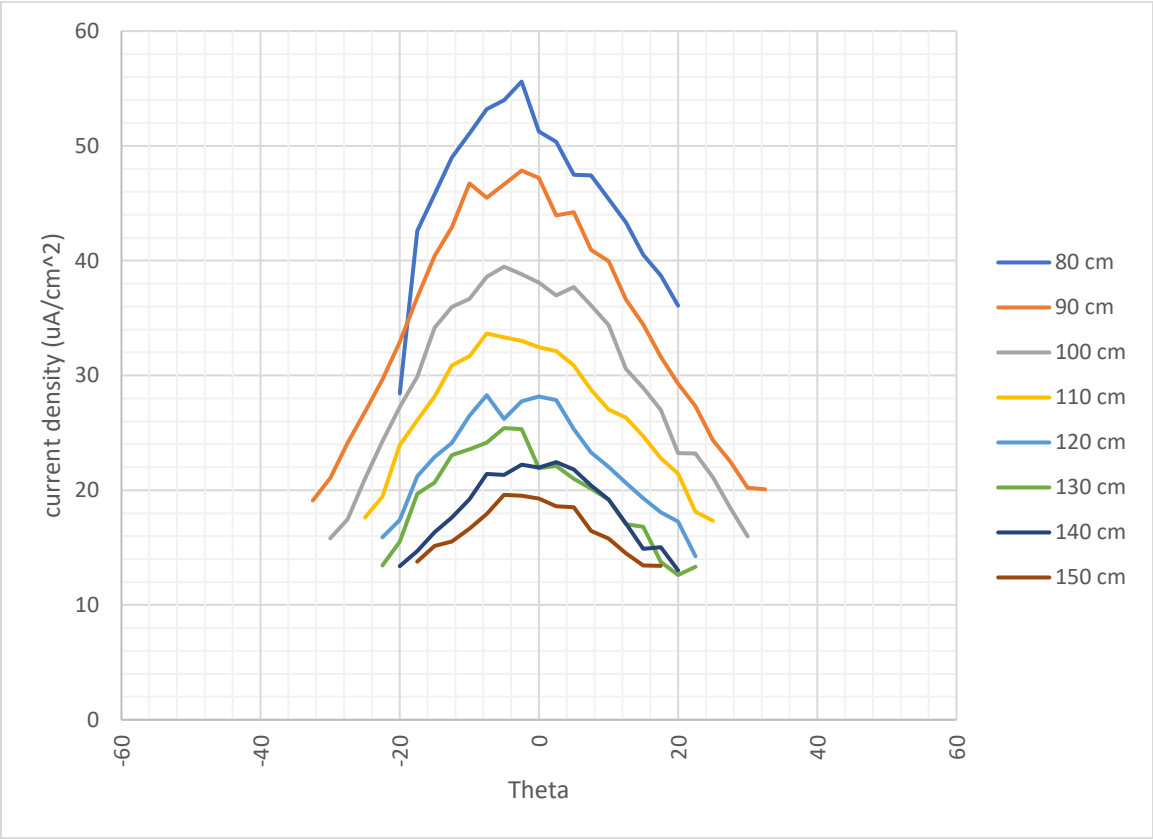

Figure 60: Elevated Faraday Probe plot

Appendix C. Projection Plot Code

```
function I6 = UnwrapperPL(Image, r_in, r_out, center, center2)

% Image=imread(Image);


[Y X z]=find(Image);

X1 = X-center(2);
Y1 = -Y+center(1);

theta=atan2(Y,X);
r = sqrt(X.^2 + Y.^2);

theta = atan2(Y1,X1);
r = sqrt(X1.^2 + Y1.^2);

rres=180;
tres=90;

% Define interpolant class
Q = scatteredInterpolant(r,theta,double(z),'natural');
% Make mesh of output image coordinates
[ri thetai] =
meshgrid(linspace(r_in,r_out,rres),linspace(pi()/2,pi(),tres));
% Map intensity values of original image to new image (using
interpolant)
Unroll = Q(ri,thetai);
%%%%% END ADAPTED SECTION %%%%

Unroll= uint8(Unroll);

I = Unroll;

%% Second 90 degrees

[ri2 thetai2] = meshgrid(linspace(r_in,r_out,rres),linspace(-pi(),-
pi()/2,tres));
% Map intensity values of original image to new image (using
interpolant)
Unroll2 = Q(ri2,thetai2);
Unroll2 = uint8(Unroll2);

I2 = Unroll2;

I3=[I;I2];

%% bottom linear section
xmin=center(2);
xmax=center2(2);
ymin=center(1);
```

```
ymax1=ymin+r_out;

xres=288;
yres=180;
Q2 = scatteredInterpolant(X,Y,double(z),'natural');

[x2, y2] =
meshgrid(linspace(xmin,xmax,xres),linspace(ymin,ymax1,yres));

Unroll3=Q2(x2,y2);
Unroll3=uint8(Unroll3');


I4=[I3;Unroll3];

%% right curved section

X2=X-center2(2);
Y2=-Y+center2(1);
theta2 = atan2(Y2,X2);
r2 = sqrt(X2.^2 + Y2.^2);


Q3 = scatteredInterpolant(r2,theta2,double(z),'natural');

[ri3 thetai3] = meshgrid(linspace(r_in,r_out,rres),linspace(-
pi()/2,pi()/2,tres*2));

Unroll4 = Q3(ri3,thetai3);
Unroll4 = uint8(Unroll4);

I5=[I4;Unroll4];

%% top linear section
ymax2=ymin-r_out;
[x3, y3] =
meshgrid(linspace(xmax,xmin,xres),linspace(ymin,ymax2,yres));

Unroll5=Q2(x3,y3);
Unroll5=uint8(Unroll5');

% figure
I6=[I5;Unroll5];
% imagesc(I6);

end


%%

%%
```

```
% oldDir=cd(strcat('C:\Users\swrig\OneDrive\AFIT\Thesis\Data\High Speed
Video\6 Jan 18 (never reached conditioned flow)\TIFF\Spoke out of
focus'));
clc
close all
clear all
% change inputs
averaging=1;
oldDir=cd(strcat('I:\video\5jan\Camera1_13_54_39'));
chanout=20;
Lycenter=102;
Lxcenter=75;
Rycenter=102;
Rxcenter=180;
testsize=UnwrapperPL(imread(strcat('Camera1_13_54_39_',num2str(1,'%03i'
),'.tiff')),0,chanout,[Lycenter,Lxcenter],[Rycenter,Rxcenter]);


Images = uint8(zeros(size(testsize,1),size(testsize,2),1020));
if averaging
    BigPicture = uint8(zeros(size(testsize,1),1020));
    avgstring = 'Pixels_condensed';
else
    avgstring = 'Full_Width';
end
%%%%%%%%%%%%%%%% Read in each frame, unroll it, add it to output image
%%%%

for i = 1:102
    % note the image may have gain applied here.
    Images(:,:,i) =
UnwrapperPL(imread(strcat('Camera1_13_54_39_',num2str(i,'%03i'),'.tiff'
)),0,chanout,[Lycenter,Lxcenter],[Rycenter,Rxcenter]);
    if ~averaging
        if i == 1
            for j = 1:size(Images,1)
                BigPicture(j,:,1) = uint8(Images(j,:,i));
            end
        else
            for j = 1:size(Images,1)
                holder(j,:) = uint8(Images(j,:,i));
            end
            BigPicture = [BigPicture holder];
        end
    elseif averaging
        for j = 1:size(Images(:,1,1))
            BigPicture(j,(i*10)-9) = uint8(mean2(Images(j,:,i)));
            BigPicture(j,(i*10)-8) = uint8(mean2(Images(j,:,i)));
            BigPicture(j,(i*10)-7) = uint8(mean2(Images(j,:,i)));
            BigPicture(j,(i*10)-6) = uint8(mean2(Images(j,:,i)));
            BigPicture(j,(i*10)-5) = uint8(mean2(Images(j,:,i)));
            BigPicture(j,(i*10)-4) = uint8(mean2(Images(j,:,i)));
            BigPicture(j,(i*10)-3) = uint8(mean2(Images(j,:,i)));
            BigPicture(j,(i*10)-2) = uint8(mean2(Images(j,:,i)));
            BigPicture(j,(i*10)-1) = uint8(mean2(Images(j,:,i)));
```

```
            BigPicture(j,(i*10)) = uint8(mean2(Images(j,:,i)));
        end
    end
end
%%%%%%%%%%%%%%%% Display and Save %%%%%%%%%%%%%%
imshow(BigPicture)
imwrite(BigPicture, strcat('13_54_39_unwrap.tiff'));
cd(oldDir);

%%

%%

color=1;
gain=1;
save=1;
oldDir=cd(strcat('I:\video\5jan\Camera1_13_54_39'));
%
%
I = gain*imread(strcat('13_54_39_unwrap.tiff'));
%
surf(I,'EdgeColor','none');
view(2);
array = 0:0.01:1;
map = [array;array;array];
colormap(map')
xlim([1,1020]);
ylim([1,936]);
ax = gca;
ax.XTick = 100:100:1000;
ax.XTickLabel = {'10','20','30','40','50','60','70','80','90','100'};
ax.YTick = [1,90,180,468,558,648,936];

ax.YTickLabel = {'90a','-180','-90a','-90b','0','90b','90a'};
xlabel('time (\mus)');
ylabel('Azimuthal position (deg)');
if color
    colormap hot
end
% title(strcat('Test45(2)'));
if save
    cd(strcat('I:\video\5jan\Camera1_13_54_39'));
    savefig(strcat('Unrolled_Plot_'));
    print(strcat('Unrolled_Plot_'),'-dtiff');
end
cd(oldDir)
```

Bibliography

1. D. M. Goebel and I. Katz, *Fundamentals of Electric Propulsion*, No. 1 in JPL Space Science and Technology Series, Wiley, Hoboken, New Jersey, 2008.

2. A. E. Gonzales, M. K. Scharfe, J. W. Koo and W. A. Hargus, "Comparison of Numerical and Experimental Time-Resolved Near-Field Hall Thruster Plasma Properties," in *AIAA Joint Propulsion Conference*, Atlanta,Georgia, July- Aug 2012.

3. R. A. Spores, R. B. Cohen, and M. Birkan, "The USAF electric propulsion program," in Proc. 25th Int. Elect. Propul. Conf., vol. 1, Worthington, OH, 1998, p. 1.

4. Chen, F. F., Introduction to Plasma Physics, Plenum, New York, New York, 1974.

5. Jahn, R. G. (2006). *Physics of electric propulsion*. Mineola, NY: Dover Pub.

6. Choueiri, E. Y., "Plasma oscillations in Hall thrusters," *Physics of Plasmas*, Vol. 8, No. 4, April 2001, pp. 1411-1426.

7. Cunningham D.A., "Localized Plasma Measurement During Instability Modes In a Hall Thruster," Air Force Institute of Technology, Wright-Patterson Air Force Base, Ohio, 2016.

8. Sekerak, M. J., *Plasma Oscillations and Operational Modes in Hall Effect Thrusters*, Ph.D. thesis, University of Michigan, Ann Arbor, Michigan, 2014.

9. G. S. Janes and R. S. Lowder, "Anomalous Electron Diffusion and Ion Acceleration in a low-density plasma," *American Institute of Physics*, vol. 9, no. 6, pp. 1115-1123, 1966.

10. Boeuf, J.-P. and Garrigues, L., "Low frequency oscillations in a stationary plasma thruster," *Journal of Applied Physics*, Vol. 84, 1998, pp. 3541.

11. Fife, J. M., Martinez-Sanchez, M., and Szabo, J., "A Numerical Study of Low-Frequency Discharge Oscillations in Hall Thrusters," Tech. Rep. AIAA-97-3051, American Institute of Aeronautics and Astronautics, Washington, D. C., 1997.

12. McDonald, M. S., A. D. Gallimore, B. A. St. Pierre and C. K. Bellant, "Measurement of Cross-Field Electron Current in a Hall Thruster Due to Rotating Spoke Instabilities," in *47th AIAA/ASME/SAE/ASEE Joint Propulsion Conference & Exhibit*, San Diego, California, 31 July - 03 August 2011.

13. Kemp, R.F., and J. M. Sellen, "Plasma Potential Measurements by Electron Emissive Probes," *Review of Scientific Instruments* , vol. 37, p. 455, 1966.

14. S. Mazouffre, A. Petin, P. Kudrna and M. Tichy, "Development of a High-Frequency Emissive Probe," *IEEE TRANSACTIONS ON PLASMA SCIENCE*, vol. 43, no. 1, 2015.

15. K. Dannenmayer, A. Bulit, and J. Amo, "Measurements of plasma parameters in the plume of electric propulsion devices – Recent works performed at the ESA Propulsion Laboratory," in *34th International Electric Propulsion Conference and 6th Nano-satellite Symposium*, Hyogo-Kobe, Japan, July2015.

16. Pote, B., Hruby, V., Tedrake, R., Performance of a Multi-Kilowatt Non-Circular Discharge Hall Thruster, AIAA-2000-3249, 36th Joint Propulsion Conference & Exhibit, Huntsville, AL, July 16-19, 2000.

17. Hruby, V., Monheiser, J., Pote, B., Rostler, P., Kolencik, J., Freeman, C., Development of Low Power Hall Thrusters, AIAA-99-3534, 30th Plasmadynamics and Lasers Conference, Norfolk, VA, June 28 - July 1, 1999.

18. Hargus, W. J., Cappelli, M., Development of a Linear Hall Thruster, AIAA-98-3336, 34th Joint Propulsion Conference and Exhibit, Cleveland, OH, July 12-15, 1998.

19. Busek Co. Inc., "BHT-400-OCD Pseudo Linear (Obround) Hall Thruster Installation and Operating Manual," Natick, 2017.

20. Busek Co. Inc., "Busek Hollow Cathode BHC-1500 Operating and Maintenance Manual," Natick, 2008.

21. Busek Co. Inc., "BHT-600-pm Permanent Magnet Hall Thruster Installation and Operating Manual," Natick, 2016.

22. B. C. Inc., "www.busek.com," 2013. [Online]. Available: http://www.busek.com/index_htm_files/70008509B.pdf.

23. N. Hyatt. Hall Effect Thruster Characterization through Potential, Magnetic, and Optical Measurements. Master's thesis, Air Force Institute of Technology, March 2017.

24. Plasma Controls, LLC, "Emissive Probe Instruction Manual," Fort Collins, 2015.

25. C. Farnell and J. D. Williams, "Faraday Probe Operating Manual," Ft. Collins.

26. D. M. Bui, "Plume Characterization of Busek 600W Hall Thruster," Air Force Institute of Technology, 2005.

27. Liu, D., *Two-Dimensional Time-Dependent Plasma Structures of a Hall Effect Thruster*, Ph.D. thesis, Air Force Institute of Technology, Wright-Patterson Air Force Base, Ohio, September 2011.

REPORT DOCUMENTATION PAGE

Form Approved
OMB No. 074-0188

PLEASE DO NOT RETURN YOUR FORM TO THE ABOVE ADDRESS.

1. REPORT DATE *(DD-MM-YYYY)*	**2. REPORT TYPE**	**3. DATES COVERED** *(From – To)*
22-03-2018	Master's Thesis	August 2016 – March 2018

TITLE AND SUBTITLE

Pseudo Linear Hall Effect Thruster Characterization Through Potential, Magnetic, and Optical Measurements

5a. CONTRACT NUMBER

5b. GRANT NUMBER

5c. PROGRAM ELEMENT NUMBER

6. AUTHOR(S)

Sheets, Braeden A., 2nd Lieutenant, USAF

5d. PROJECT NUMBER

5e. TASK NUMBER

5f. WORK UNIT NUMBER

7. PERFORMING ORGANIZATION NAMES(S) AND ADDRESS(S)
Air Force Institute of Technology
Graduate School of Engineering and Management (AFIT/ENY)
2950 Hobson Way, Building 640
Wright-Patterson AFB OH 45433-7765

8. PERFORMING ORGANIZATION REPORT NUMBER

AFIT-ENY-MS-18-M-293

9. SPONSORING/MONITORING AGENCY NAME(S) AND ADDRESS(ES)
Air Force Office of Scientific Research Energy
Attn: Dr. Mitat Birkan
875 N. Randolph, Ste 325
Arlington, VA 22203
mitat.birkan@us.af.mil

10. SPONSOR/MONITOR'S ACRONYM(S)
AFOSR

11. SPONSOR/MONITOR'S REPORT NUMBER(S)

12. DISTRIBUTION/AVAILABILITY STATEMENT
DISTRUBTION STATEMENT A. APPROVED FOR PUBLIC RELEASE; DISTRIBUTION UNLIMITED.

13. SUPPLEMENTARY NOTES
This material is declared a work of the U.S. Government and is not subject to copyright protection in the United States.

14. ABSTRACT

Electric propulsion systems are a more mass efficient method for providing a change in velocity, ΔV, to on-orbit spacecraft, than their chemical counterparts. In comparison, electric systems generally have a much higher specific impulse, Isp, than chemical systems. One option within the realm of electric propulsion is Hall Effect Thrusters, which have moderately high specific impulse values. From their advent in the 1960s, Hall Effect Thrusters have been used for orbit station keeping, attitude control, and orbit transfer. Although the discharge cavity is conventionally circular, pseudo-linear or racetrack shaped cavities have been developed. Even though Hall thrusters have decades of flight heritage, there are still many plasma behavioral characteristics which are still unknown. Multiple non-intrusive measurement techniques were used to investigate plasma behavior both in the plume and in the channel of a pseudo linear Hall thruster. Through the visible emissions captured by a high-speed camera, breathing mode characteristics were induced and analyzed. Spoke structures were observed in only certain parts of the thruster channel. Additionally, the plume divergence was characterized by use of a Faraday probe along two axes of the thruster, indicating significantly different "keep out" regions for potential thruster use on spacecraft. Also, an irregularity was observed in the channel of the pseudo-linear thruster, which potentially could affect the lifespan of the thruster.

15. SUBJECT TERMS
Hall Thruster, Hall Effect Thruster, Electric Propulsion, Ion, Frequency Analysis , Plasma,

16. SECURITY CLASSIFICATION OF:			**17. LIMITATION OF ABSTRACT**	**18. NUMBER OF PAGES**	**19a. NAME OF RESPONSIBLE PERSON**
a. REPORT	**b. ABSTRACT**	**c. THIS PAGE**			Dr. Carl Hartsfield, AFIT/ENY
U	**U**	**U**	**UU**	93	**19b. TELEPHONE NUMBER** *(Include area code)* (937) 255-3636, ext 4667 Carl.hartsfield@afit.edu

Standard Form 298 (Rev. 8-98)
Prescribed by ANSI Std. Z39-18